MIT JOINT PROGRAM
SCIENCE POLICY
GLOBAL CHANGE

Report 325
February 2018

Description and Evaluation of the MIT Earth System Model (MESM)

Andrei Sokolov, David Kicklighter, Adam Schlosser, Chien Wang, Erwan Monier, Benjamin Brown-Steiner, Ron Prinn, Chris Forest, Xiang Gao, Alex Libardoni and Sebastian Eastham

MIT Joint Program on the Science and Policy of Global Change combines cutting-edge scientific research with independent policy analysis to provide a solid foundation for the public and private decisions needed to mitigate and adapt to unavoidable global environmental changes. Being data-driven, the Joint Program uses extensive Earth system and economic data and models to produce quantitative analysis and predictions of the risks of climate change and the challenges of limiting human influence on the environment—essential knowledge for the international dialogue toward a global response to climate change.

To this end, the Joint Program brings together an interdisciplinary group from two established MIT research centers: the **Center for Global Change Science (CGCS)** and the **Center for Energy and Environmental Policy Research (CEEPR)**. These two centers—along with collaborators from the Marine Biology Laboratory (MBL) at Woods Hole and short- and long-term visitors—provide the united vision needed to solve global challenges.

At the heart of much of the program's work lies MIT's Integrated Global System Model. Through this integrated model, the program seeks to discover new interactions among natural and human climate system components; objectively assess uncertainty in economic and climate projections; critically and quantitatively analyze environmental management and policy proposals; understand complex connections among the many forces that will shape our future; and improve methods to model, monitor and verify greenhouse gas emissions and climatic impacts.

This reprint is intended to communicate research results and improve public understanding of global environment and energy challenges, thereby contributing to informed debate about climate change and the economic and social implications of policy alternatives.

—Ronald G. Prinn and John M. Reilly,
Joint Program Co-Directors

MIT Joint Program on the Science and Policy of Global Change

Massachusetts Institute of Technology
77 Massachusetts Ave., E19-411
Cambridge MA 02139-4307 (USA)

T (617) 253-7492 **F** (617) 253-9845
globalchange@mit.edu
http://globalchange.mit.edu/

GLOBAL CHANGE

FEBRUARY 2018

Description and Evaluation of the MIT Earth System Model (MESM)

Andrei Sokolov[1,6], David Kicklighter[2], Adam Schlosser[1], Chien Wang[1], Erwan Monier[1], Benjamin Brown-Steiner[1,3], Ron Prinn[1], Chris Forest[4], Xiang Gao[1], Alex Libardoni[4] and Sebastian Eastham[5]

Abstract: The MIT Integrated Global System Model (IGSM) is designed for analyzing the global environmental changes that may result from anthropogenic causes, quantifying the uncertainties associated with the projected changes, and assessing the costs and environmental effectiveness of proposed policies to mitigate climate risk. The IGSM consists of the MIT Earth System Model of intermediate complexity (MESM) and the Economic Projections and Policy Analysis (EPPA) model. This paper documents the current version of the MESM, which includes a 2-dimensional (zonally averaged) atmospheric model with interactive chemistry coupled to the Global Land System model and an anomaly-diffusing ocean model.

1 Joint Program on the Science and Policy of Global Change, Massachusetts Institute of Technology, Cambridge, MA, USA

2 The Ecosystems Center, Marine Biological Laboratory, Woods Hole, MA, USA

3 Currently at Atmospheric and Environmental Research, Lexington, MA, USA

4 Department of Meteorology & Earth and Environmental Systems Institute, Pennsylvania State University, University Park, PA, USA

5 Laboratory for Aviation and the Environment, Department of Aeronautics and Astronautics, Massachusetts Institute of Technology, Cambridge, MA, USA

6 Corresponding author: Andrei Sokolov (sokolov@mit.edu)

1. Introduction

There is significant uncertainty in projections of future climate associated with uncertainty in possible pathways of economic development and corresponding anthropogenic emissions of different gases as well as with uncertainty in climate system response to these emissions. Climate system properties that determine its response to transient forcing, such as climate sensitivity and the rate at which the deep ocean absorbs heat simulated by atmosphere-ocean general circulation models (AOGCMs, e.g. Andrews *et al.*, 2013; Forster *et al.*, 2013; IPCC, 2013); and the strength of the carbon cycle and carbon-climate feedbacks, simulated by Earth System Models (ESMs, Friedlingstein *et al,* 2006 and 2014) differ significantly leading to a large spread in the future atmospheric CO_2 concentration and radiative forcing for a given emission scenario. There are additional uncertainties in the forcing itself, especially in the forcing associated with aerosol-cloud interaction.

Unfortunately, the available directly-measured ocean, land and atmospheric data can only place limited constraints on these key quantities (e.g. Andronova & Schlesinger, 2001; Gregory *et al.*, 2002; Forest *et al.*, 2008, Libardoni and Forest, 2011). Thus, these uncertainties have not been reduced over the last few decades in spite of significant efforts and are unlikely to be substantially reduced within the next decade or more, when important policy choices must nevertheless be made. These uncertainties, in turn, result in a rather wide uncertainty in projected future climate change.

To place our current understanding of potential future climate change within the context of these uncertainties to policy-makers and the general public, the latest report of Intergovernmental Panel on Climate Change (IPCC, 2013) provides mean values and probability intervals for projected changes of future climate, based on a multi-model ensemble (MME). There are, however, well known problems with MMEs, such as small sample size and the fact that different modes are neither independent nor likely plausible (IPCC, 2013 and literature referenced there). In addition, there are no guaranties that the existing AOGCMs and ESMs sample the full ranges of uncertainties in different climate characteristics and moreover sample these ranges homogeneously. An alternative approach is to estimate the probability distributions of climate parameters based on available data for past climate and then carry out large (few hundred members) ensembles of future climate simulations by sampling parameter values from these distributions.

Even with much greater computational power than is available today, however, it will not be possible to carry out such an exercise using a fully complex state-of-the-art AOGCM or ESM. Therefore, such studies are usually carried out with Earth System Models of Intermediate Complexity (EMICs) (Knutti *et al.*, 2003; Rogelj *et al.*, 2012; Sokolov *et al,* 2009; Webster *et al.*, 2003 and 2012). It has been shown that, with an appropriate choice of parameter values EMICs can reproduce global mean changes simulated by different AOGCMs and ESMs under different forcing scenarios (Raper *et al.*, 2001; Sokolov *et al.*, 2003; Meinshausen *et al.* 2011). Model intercomparisons also have shown that in many cases changes in climate predicted by models of intermediate complexity are very similar to those obtained in the simulations with AOGCMs (Gregory *et al.*, 2005; Stouffer *et al.*, 2005).

The MIT Earth System Model (MESM) is designed to provide the flexibility and computational speed required to handle uncertainty analysis while representing to the best degree possible the physics, chemistry and biology of the more computationally intensive AOGCMs. Within the MIT Integrated System Model (IGSM), the MESM is linked to a model of human interactions so that the consequences of various economic and policy decisions on future climate may be evaluated. The MESM can be run in both concentration-driven and emissions-driven modes. As a result, it can be used to quantify uncertainties in future climate. To do this, the MESM is first used to produce probability distributions for the climate sensitivity, the rate of heat uptake by the deep oceans, and the net forcing due to aerosol-radiation interaction by comparing observed temperature changes over the 20th century with the results of historical (concentration-driven) simulations in which model parameter values were varied over wide ranges (Forest *et al.*, 2002 and 2008; Libardoni and Forest 2011 and 2013; Libardoni 2017). The constructed distributions are then used to carry out ensembles of future climate emissions-driven simulations and produce probability distributions for changes in different climate variables. Uncertainty in climate system response are then combined with uncertainty in anthropogenic emissions (Webster *et al.*, 2002 and 2008) to estimate overall uncertainty in possible anthropogenic climate change (Sokolov *et al.*, 2009; Webster *et al.*, 2003 and 2012). In previous publications acronym "IGSM" was used for both Integrated System Model as a whole and its climate component. Here we use acronym "MESM" for the latter.

The first version of the MESM was developed in the mid-1990s (Sokolov and Stone 1995 and 1997; Prinn *et al.*, 1999) and has since been continually modified and extended (Sokolov *et al.*, 2005). Different versions of the MESM were used in a number of model intercomparison projects (e.g., Gregory *et al.*, 2005; Petoukhov *et al.*, 2005; Stouffer *et al.*, 2005; Brovkin *et al.*, 2006; Plattner *et al.*, 2008; Eby *et al.*, 2013; Olsen *et al.* 2013; Zickfeld *et al.*, 2013; Brasseur *et al.*, 2016). The MESM shows generally comparable results to those of more complex models. For example, the study of the impact of aviation emissions on atmospheric chemical composition and climate showed

that MESM performs within the envelope of the more complex 3-D chemistry-climate models (Brasseur *et al.*, 2016; Olsen *et al.*, 2013).

In this paper, we describe the current version of the MESM, as of the middle of 2017. Description of the model components is given in Section 2. Section 3 provides a comparison of simulated present-day climate and historical climate change with results produced by CMIP5 models and available observations.

2. Model Description

The major model components of the MESM (**Figure 1**) include:

- An atmospheric dynamics, physics and chemistry model, which includes a sub-model of urban chemistry,
- An ocean model with carbon cycle and sea-ice sub-models,
- A linked set of coupled process-based land models, the Terrestrial Ecosystem Model (TEM), a fully integrated Natural Emissions Model (NEM), and the Community Land Model (CLM), that simulate terrestrial water, energy, carbon and nitrogen budgets including carbon dioxide (CO_2) and trace gas emissions of methane (CH_4) and nitrous oxide (N_2O).

The earth system depicted in Figure 1 represents a fully coupled system that allows simulation of critical feedbacks among its components. Time-steps used in the various sub-models range from 10 minutes for atmospheric dynamics, to 1 month for TEM, reflecting differences in the characteristic time-scales of different processes simulated by the MESM. The major model components of the MESM and linkages are summarized below.

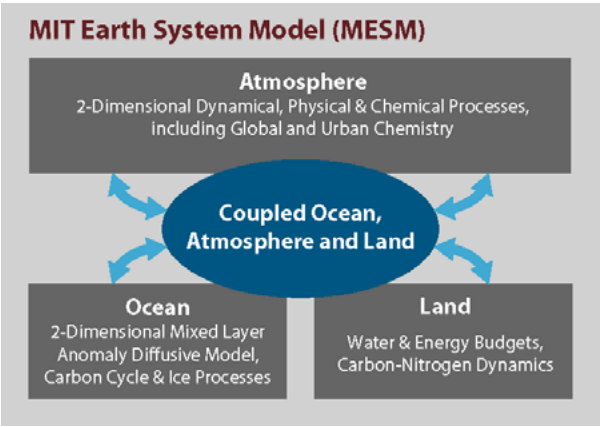

Figure 1. MIT Earth System Model of Intermediate Complexity (MESM)

2.1 Atmospheric Dynamics and Physics

The MIT two-dimensional (2D) atmospheric dynamics and physics model (Sokolov & Stone, 1998) is a zonally-averaged statistical dynamical model that explicitly solves the primitive equations for the zonal mean state of the atmosphere and includes parameterizations of heat, moisture, and momentum transports by large-scale eddies based on baroclinic wave theory (Stone & Yao, 1987, 1990). The model's numerics and parameterizations of physical processes, including clouds, convection, precipitation, radiation, boundary layer processes, and surface fluxes, build upon those of the Goddard Institute for Space Studies (GISS) GCM (Hansen *et al.*, 1983). The radiation code includes all significant greenhouse gases (H_2O, CO_2, CH_4, N_2O, CFCs and O_3) and multiple types of aerosols. The model's horizontal and vertical resolutions are variable, but in the standard version of MESM it has 4° resolution in latitude and eleven levels in the vertical.

The MIT 2D atmospheric dynamics and physics model allows up to four different types of surfaces in the same grid cell (ice-free ocean, sea-ice, land, and land-ice). The surface characteristics (e.g., temperature, soil moisture, albedo) as well as turbulent and radiative fluxes are calculated separately for each kind of surface while the atmosphere above is assumed to be well mixed horizontally in each latitudinal band. The area weighted fluxes from different surface types are used to calculate the change of temperature, humidity, and wind speed in the atmosphere. Fluxes of sensible heat and latent heat are calculated in the atmospheric model by bulk formulas with turbulent exchange coefficients dependent on the Richardson number. The atmosphere's turbulence parameterization is also used in the calculation of the flux derivatives with respect to surface temperature. To account for partial adjustment of near surface air temperature to changes in fluxes, the derivatives are calculated under the assumption that the exchange coefficients are fixed. A more detailed discussion of the technical issues involved in the calculations of these fluxes and their derivatives is given in Kamenkovich *et al.* (2002).

The moist convection parameterization, which was originally designed for the GISS Model I (Hansen *et al.* 1983), requires knowledge of sub-grid scale temperature variance. Zonal temperature variance associated with transient eddies is calculated using a parameterization proposed by Branscome (see Yao and Stone 1987). The variance associated with stationary eddies is represented by adding a fixed variance that follows more closely the climatological pattern (see Figure. 7.8b of Peixoto and Oort 1992). In addition, the threshold values of relative humidity for the formation of large-scale cloud and precipitation varies with latitude to account for the dependence of the zonal variability of relative humidity on latitude. Zonal precipitations simulated by the atmospheric model are partitioned into land and

ocean components using present day climatology. These changes led to an improvement in the zonal pattern of the annual cycle of land precipitation and evapotranspiration (Schlosser at al. 2007).

The atmospheric model's climate sensitivity can be changed by varying the cloud feedback. Namely, the cloud fraction used in radiation calculation (C^{rad}) is adjusted as follows:

$$C^{rad} = C^{o} \cdot (1.0 + \kappa \cdot \Delta T_{srf}), \quad (1)$$

where C^{o} is a cloud fraction simulated by the model, ΔT_{srf} is a difference of the global-mean surface air temperature from is values in the control climate simulation and κ is a parameter used to vary climate sensitivity.

This method was proposed by Hansen *et al.* (1993) and was extensively tested in simulations with the MIT climate model (Sokolov & Stone, 1998). The choice of cloud feedback seems very natural because differences in climate sensitivity between different AOGCMs are to large extent caused by large differences in this feedback (Cess *et al.* 1990; Colman 2003; Bony *et al.* 2006; Webb *et al.* 2006; Williams *et al.* 2006). The method was later modified by using κ of different signs for high and low clouds (Sokolov, 2006), accounting for the fact that the feedback associated with changes in cloud cover has different signs for high and low clouds. Therefore, using different signs in Equation 1 depending on cloud heights minimizes the value of κ required to obtain a specific value of climate sensitivity. In addition, the use of the modified method improves the agreement in simulated changes is surface fluxes between the MIT climate model and different AOGCMs. This approach to changing climate sensitivity was also tested in simulations with CAM3 (Sokolov and Monier, 2012), by comparison with perturbed physics approach.

2.2 Urban and Global Atmospheric Chemistry

To calculate atmospheric composition, the model of atmospheric chemistry includes the climate-relevant chemistry of gases and aerosols at two domains: the urban scale and the global scale. The urban model is a sub-grid scale chemistry model whose emissions and pollutants are exported (along with emissions from non-urban areas) into the 2D global zonal-mean model of atmospheric chemistry, which is linked to the atmospheric dynamics and physics model described above. This atmospheric model provides wind speeds, temperatures, solar radiation fluxes, and precipitation to both the urban and global scale chemistry models. The details of the sub-grid scale urban chemistry model and the 2D zonal-mean atmospheric chemistry model, and their coupling, are described below.

2.2.1 Urban Atmospheric Chemistry

Urban emissions and air pollution have a significant impact on global methane, ozone, and aerosol chemistry, and thus on the global climate. However, the nonlinearities in the chemistry cause urban emissions to undergo different net transformations than rural emissions, and thus urban chemistry is treated separately from non-urban emissions within the MESM. Accuracy in describing these transformations is necessary because the atmospheric lifecycles of exported air pollutants such as CO, O_3, NO_x and VOCs, and the climatically important species CH_4 and sulfate aerosols, are linked through the fast photochemistry of the hydroxyl free radical (OH) as we will emphasize in the results discussed later in section 5. Urban air-shed conditions need to be resolved at varying levels of pollution. The urban air chemistry model must also provide detailed information about particulates and their precursors important to air chemistry and human health, and about the effects of local topography and structure of urban development on the level of containment and thus the intensity of air pollution events. This is an important consideration because air pollutant levels are dependent on projected emissions per unit area, not just total urban emissions.

The urban atmospheric chemistry model has been introduced as an additional component to the original global model (Prinn *et al.* 1999) in MESM (Calbo *et al.* 1998; Mayer *et al.* 2000; Prinn *et al.* 2007). It was derived by fitting multiple runs of the detailed 3D California Institute of Technology (CIT) Urban Airshed Model, adopting the probabilistic collocation method to express outputs from the CIT model in terms of model inputs using polynomial chaos expansions (Tatang *et al.* 1997). This procedure results in a reduced format model to represent about 200 gaseous and aqueous pollutants and associated reactions over urban areas that is computationally efficient enough to be embedded in the global model. The urban module is formulated to take meteorological parameters including wind speed, temperature, cloud cover, and precipitation as well as urban emissions as inputs. Calculated with a daily time step, it exports fluxes along with concentrations (peak and mean) of selected pollutants to the global model.

2.2.2 Global Atmospheric Chemistry

The 2D zonal mean model that is used to calculate atmospheric composition is a finite difference model in latitude-pressure coordinates, and the continuity equations for the trace constituents are solved in mass conservative, of flux, form (see Wang *et al.*, 1998 for a more complete description). The model includes 33 chemical species with 41 gas-phase and 12 aqueous-phase reactions (Wang *et al.*, 1998). For the longer-lived species ($CFCl_3$, CF_2CL_2, N_2O, CO, CO_2, NO, NO_2, N_2O_5, HNO_3, CH_4, CH_2O, SO_2, H_2SO_4, HFC, PFC, SF_6, and black carbon and organic carbon aerosols), the chemistry model includes convergence due to transport, parameterized north-south eddy transport, convective transport, and local true production and loss due to surface emissions, deposition, and chemical reaction.

For the very-reactive atoms (e.g. O), free radicals (e.g. OH), and molecules (e.g. H_2O_2), their concentrations are unaffected by transport due to their very short lifetimes, and only their chemical production and loss (in both the gaseous and aqueous phase) is considered. The scavenging of carbonaceous and sulfate aerosol species by precipitation is also included using a method based on a detailed 3D climate-aerosol-chemistry model (Wang, 2004). Water vapor and air (N_2 and O_2) mass densities are computed using full continuity equations as part of the atmospheric dynamics and physics model (described above) to which the chemical model is coupled.

2.2.3 Coupling of Urban and Global Atmospheric Chemistry

The urban chemistry module was derived based on an ensemble of 24-hour long CIT model runs and thus is processed in the IGSM with a daily time step, while the global chemistry module is run in a real time step with the dynamics and physics model, 20 minutes for advection and scavenging, 3 hours for tropospheric reactions. The two modules in the IGSM are processed separately at the beginning of each model day, supplied by emissions of non-urban and urban regions, respectively. At the end of each model day, the predicted concentrations of chemical species by the urban and global chemistry modules are then remapped based on the urban to non-urban volume ratio at each model grid. Beyond this step, the resultant concentrations at each model grid will be used as the background concentration for the next urban module prediction and also as initial values for the global chemistry module (Mayer *et al.* 2000).

2.3 Ocean Component

The ocean model used in the version of MESM described in this paper, consists of a mixed-layer model with a horizontal resolution of 4° in latitude and 5° in longitude and a 3000-m deep anomaly-diffusing ocean model beneath. Mixed-layer depth is prescribed based on observations as a function of time and location (Hansen *et al.*, 1983). In addition to the temperature of the mixed layer, the model also calculates the average temperature of the seasonal thermocline and the temperature at the annual maximum mixed layer depth (Russell *et al.* 1985). Heat mixing into the deep ocean is parametrized by the diffusion of the difference of the temperature at the bottom of the seasonal thermocline from its value in a pre-industrial climate simulation (Hansen *et al.* 1984; Sokolov and Stone 1998). Since this diffusion represents a cumulative effect of heat mixing by all physical processes, the values of the diffusion coefficients are significantly larger than those used in the sub-grid scale diffusion parameterizations in ocean global circulation modesl (OGCMs). The spatial distribution of the diffusion coefficients used in the diffusive model is based on observations of tritium mixing into the deep ocean (Hansen *et al.* 1988). The rate of oceanic heat uptake is varied by multiplying diffusion coefficients by the same factor in all locations.

The coupling between the atmospheric and oceanic models takes place every hour. The heat flux (FH) at the longitude-latitude point (i,j) is calculated as:

$$FH(i,j) = FHZ(j) + \partial FHZ/\partial T\,(j) * (Ts(i,j) - Tsz(j)), \quad (2)$$

where FHZ (j) and $\partial FHZ/\partial T$ (j) are zonally averaged heat flux and its derivative with respect to surface temperature, and $Ts(i,j)$ and $Tsz(j)$ are surface temperature and its zonal mean.

The mixed-layer model also includes specified vertically-integrated horizontal heat transport by the deep oceans, a so-called "Q-flux". This flux has been calculated from a simulation in which sea surface temperature and sea-ice distribution were relaxed toward their present-day climatology with relaxation a coefficient of 300 Wm^{-2}/K, corresponding to an e-folding time-scale of about 15 days for the 100 m deep mixed-layer. Relaxing SST and sea ice on such a short time scale, while being virtually identical to specifying them, avoids problems with calculating the Q-flux near the sea ice edge.

A thermodynamic ice model is used for representing sea ice. The model has two layers and computes ice concentration (the percentage of area covered by ice) and ice thickness.

An alternative version of MESM was developed by replacing simplified ocean model with the MIT 3D OGCM (Dutkiewicz *et al.*, 2005). A detailed comparison of the results of simulations with the two versions of the MESM was carried out to evaluate the performance of the anomaly diffusing ocean model (ADOM) on different time scales Sokolov *et al.* (2007). This comparison led to significant modification of the ocean carbon model originally used in AODM (Holian *et al.* 2001). In the current version of MESM, the formulation of carbonate chemistry and parameterization of air-sea carbon fluxes are similar to the ones used in the MIT 3D OGCM (Dutkiewicz *et al.*, 2005).

Vertical and horizontal transports of the total dissolved inorganic carbon, though, are parameterized by diffusive processes. The values of the horizontal diffusion coefficients are taken from Stocker *et al.* (1994), and the coefficient of vertical diffusion of carbon (K_{vc}) depends on the coefficient of vertical diffusion of heat anomalies (K_v). Originally, K_{vc} was assumed to be proportional to K_v (Prinn *et al.* 1999; Sokolov *et al.* 1998). This assumption, however, does not take into account the vertical transport of carbon due to

the biological pump. In the present version of MESM, Kvc is, therefore, defined as:

$$K_{vc} = K_{vco} + rK_v \quad (3)$$

Where K_{vco} represents mixing due to the biological pump and rKv due to physical processes. Values of K_{vco} and r are chosen based on comparison with results obtained in simulations with MIT 3D OGCM and observations (see section 3.1). Because K_{vco} is a constant, the vertical diffusion coefficients for carbon have the same latitudinal distribution as the coefficients for heat anomalies. For simulations with different rates of oceanic uptake, the diffusion coefficients are scaled by the same factor in all locations. Therefore, rates of both heat and carbon uptake by the ocean are defined by the global mean value of the diffusion coefficient for heat. In the rest of the paper the symbol Kv is used to designate the global mean value.

Comparisons with 3D ocean simulations have shown that the assumption that changes in ocean carbon can be simulated by the diffusive model with fixed diffusion coefficient works only for about 150 years. On longer timescales, the simplified carbon model overestimates the ocean carbon uptake. However, if Kvc is assumed to be time dependent, the MESM reproduces changes in ocean carbon as simulated by the 3D OGCM on multi century scales (Sokolov *et al.* 2007). Thus, for the runs discussed here, the coefficient for vertical diffusion of carbon was calculated as:

$$K_{vc}(t) = (K_{vco} + rK_v) \cdot f(t) \quad (4)$$

Where f(t) is a time dependent function constructed based on the analyses of the depths of carbon mixing in simulations with the 3D OGCM.

Overall results presented by Sokolov *et al.* (2007) show that in spite of its inability to depict feedbacks associated with the changes in the ocean circulation and a very simple parameterization of the ocean carbon cycle, the version of the MESM with the ADOM is able to reproduce the important aspects of the climate response simulated by the version with the OCGM through the 20th and 21st century and can be used to produce probabilistic projections of changes in many of the important climate variables, such as surface air temperature and sea level, through the end of 21st century.

The MESM also has been shown, with an appropriate choice of the model's cloud feedback and effective diffusion coefficients, to reproduce the transient surface warming and sea level rise due to thermal expansion of the ocean as calculated in various coupled AOGCMs for 120–150 year time-scales (Sokolov & Stone, 1998; Sokolov *et al.*, 2003).

2.4 Land Component

The land component of the MESM estimates how fluxes of heat, water, carbon and nitrogen, both within land ecosystems and between land and the atmosphere, vary across the globe over time. In addition, the land component estimates how soil moisture and the storage of carbon and nitrogen in vegetation and soils vary across the globe over time. The land fluxes and storages are estimated based on values of near-surface atmospheric states (e.g. air temperature, humidity, pressure, wind speed) and fluxes (radiation, precipitation), as well as atmospheric chemistry (carbon dioxide, ozone), determined by the atmospheric component of the MESM along with external data sets that prescribe the distribution of land cover and soil texture across the globe. The land component estimates of albedo, sensible heat, latent heat, evapotranspiration, and fluxes of carbon dioxide (CO_2), methane (CH_4), and nitrous oxide (N_2O) are then used by the atmospheric component of the MESM to determine changes in atmospheric physics and chemistry. In order to assess the value of global land resources, estimates of net primary production (NPP) are used by the EPPA model in the MIT IGSM to indicate how this ecosystem service influences economic activity.

Global processes in the land component are represented with a dynamically linked set of terrestrial biogeophysical (*i.e.*, water and energy budgets) and biogeochemical (*i.e.*, carbon and nitrogen budgets including carbon dioxide, methane, and nitrous oxide fluxes) sub-models. These biogeophysical and biogeochemical calculations are organized into a single, self-consistent framework for the global terrestrial environment and hereafter referred to as the Global Land Systems (GLS) framework (Schlosser *et al.* 2007). The GLS framework, employs three coupled sub-models to represent the terrestrial water, energy, and ecosystem processes:

- The Community Land Model (CLM) described by Bonan *et al.* (2002) calculates the global, terrestrial water and energy balances.
- The Terrestrial Ecosystems Model (TEM) of the Marine Biological Laboratory (Melillo *et al.*, 1993, 2009; Xiao *et al.*, 1997, 1998; Tian *et al.*, 1999; Felzer *et al.*, 2004) simulates carbon and nitrogen fluxes and the storage of carbon and nitrogen in vegetation and soils including the uptake and release of CO_2 associated with NPP, decomposition and carbon sequestration or loss.
- The Natural Emissions Model (NEM) described by Liu (1996) and Prinn *et al.* (1999) simulates CH_4 and N_2O fluxes.

Water, energy and carbon are conserved among these sub-models. The GLS is also designed to be flexible and runs either with the meridional resolution (4˚) of the zonally-averaged atmospheric model within the MESM, or over a

latitude-longitude grid for targeted studies (*e.g.*, 2˚ by 2˚ as in Gao *et al.* 2013, and 0.5˚x0.5˚ as in Melillo *et al.*, 2009).

Herein, we describe the coupled configuration of the GLS used within the MESM. In this GLS configuration, a vegetation mosaic scheme has been used to represent the distribution of vegetation within a latitudinal zonal band at the same spatial resolution for all submodels. Each latitudinal band is represented with a mosaic of 35 land cover or IGSMVEG types (Schlosser *et al.*, 2007) based on the presence or absence of a dominant tree, shrub or grass cover, ecological region (*i.e.*, boreal, temperate, tropical), moisture status (upland, floodplain or wetland) and land management (crop, pasture). In most applications of the GLS within the MESM, the land cover has been assumed to be potential vegetation (*i.e.*, natural vegetation in the absence of human activity) such that the potential impacts of land-use change on the ability of land to store carbon and nitrogen have not been considered. However, a scheme for incorporating the influence of land-use change on land carbon dynamics in the GLS has been developed and applied in Eby *et al.* (2013) and Zickfeld *et al.* (2013).

Below we highlight the key features of each of the land sub-models and modifications made to these sub-models for their implementation in the MESM.

2.4.1 The Community Land Model (CLM)

As in previous implementations of land biogeophysical and hydrologic processes within the IGSM framework, we have drawn from the Community Land Model (CLM, Lawrence *et al.*, 2011). The CLM has been developed from a multi-institutional collaboration of land models, and serves as the core land system model for energy, water, carbon, and nutrient cycle studies within the Community Earth System Model (Oleson *et al.*, 2010). CLM has also been widely used and documented in land data assimilation research (*e.g.,* Zhang *et al.*, 2012), hydrologic studies at the global (e.g. Pu *et al.*, 2012), regional (e.g. Swenson *et al.*, 2012; Zampieri *et al.*, 2012), and river-basin (e.g. Vano *et al.*, 2012) scales, as well as coupled climate prediction studies (*e.g.,* Tseng *et al.*, 2012; Xin *et al.*, 2012). CLM is also benchmarked within the iLAMB framework (e.g. Randerson *et al.*, 2009).

Within current version of MESM, we have employed CLM Version 3.5 that largely follows the detailed documentation provided by Oleson *et al.* (2010) as well as many of the features highlighted by Lawrence *et al.* (2011). We however have made some modifications to CLM's configuration used within the MESM. Within CLM's surface soil hydrologic formulation, infiltration of rainfall in the uppermost layer of the soil required further refinement for its implementation in MESM. In the initial testing of CLM within the MESM's zonal configuration, it was found that CLM produced excessive infiltration into the soil column. This resulted in an appreciably low bias in runoff and subsequently an excessive amount of evapotranspiration as compared to our previous versions of CLM implemented in the model and also against a multi-model consensus of estimates (Schlosser *et al.*, 2007 – see Fig. 15). The algorithm that describes the infiltration rate, q_{inmax}, into the uppermost soil layer can be summarized as:

$$q_{inmax} \sim \left(1 - \frac{2b\psi_{sucsat}}{dz}\right) * F_{dry} * K_{sat} \quad (5)$$

where b is the Clapp-Hornberger parameter, ψ_{sucsat} is the soil suction from the top layer of soil, dz is the thickness of the top soil layer, F_{dry} is a dryness factor of the upper soil layer, and K_{sat} is the saturated hydraulic conductivity. This infiltration formulation closely follows that of the classic Green-Ampt formulation (1911) for "enhanced" (i.e. values greater than saturated hydraulic conductivity) infiltration rate for dry soils—and will sustain this condition for dry soils (i.e. sub-saturated) in the uppermost soil layer. The inherent assumption with this formulation is that saturated and unsaturated conditions in the uppermost soil layer will occur sporadically over a large heterogeneous landscape of intermittent precipitation. However, within our zonally resolved implementation of CLM, we have removed this enhancement effect. While the MESM does resolve the temporal episodic nature of precipitation provided to the GLS (see Schlosser *et al.*, 2007)—the spatially heterogeneous nature of these conditions is not comprehensively resolved. Therefore, we simply set the maximum infiltration rate equal to saturated hydraulic conductivity. As a result of this modification, we find that our estimates of runoff and subsequent evapotranspiration are more aligned with present-day estimates from the more detailed models—judged commensurately on a zonally averaged basis (discussed in Section 3.3).

The CLM, as well as atmospheric physics, is run at an hourly time scales in order to resolve diurnal variations in the surface energy budget and associated radiative and turbulent heat exchange as well as momentum flux between the land and atmosphere. All inputs to CLM that require a temporal sampling resolution at the time-step are provided by the atmospheric model (as shown in Figure 1); CLM then calculates surface heat, water and momentum fluxes that are passed back to the atmospheric model. The calculations of soil/vegetation water and energy states and fluxes (and corresponding storages and temperatures) are averaged and accumulated as necessary given the time-steps of TEM and NEM. CLM provides estimates of soil moisture and temperature profiles, as well as evapotranspiration rates that are required inputs for the TEM and NEM components and used to estimate fluxes of CO_2, N_2O and CH_4 between terrestrial ecosystems and the atmosphere.

2.4.2 The Terrestrial Ecosystems Model (TEM)

The Terrestrial Ecosystem Model (TEM) is a process-based biogeochemistry model that uses spatially referenced information on atmospheric chemistry, climate, elevation, soil texture, and land cover to estimate monthly fluxes and pool sizes of carbon, nitrogen and water among vegetation, soils and the atmosphere. The TEM is well documented and has been used to examine patterns of land carbon dynamics across the globe including how they are influenced by multiple factors such as CO_2 fertilization, ozone pollution, climate change and variability, and land-use change, (Felzer *et al.*, 2004, 2005; Reilly *et al.*, 2007, 2012; Sokolov *et al.*, 2008; Melillo *et al.*, 2009, 2016; Galford *et al.* 2010, 2011; Kicklighter *et al.* 2012, 2014).

In TEM, the uptake of atmospheric carbon dioxide by vegetation, also known as gross primary production or GPP is dependent upon photosynthetically active radiation (PAR), leaf phenology, air temperature, evapotranspiration rates, atmospheric concentrations of carbon dioxide and ozone, the availability of inorganic nitrogen in the soil, and the ratio of carbon to nitrogen (C:N) of new plant biomass (Raich *et al.* 1991; McGuire *et al.* 1997; Tian *et al.* 1999; Felzer *et al.* 2004). Carbon dioxide is released back to the atmosphere from terrestrial ecosystems as a result of the autotrophic respiration (R_A) of plants and the heterotrophic respiration (R_H) associated with the decomposition of detritus. Net primary production (NPP), which is an important source of food and fiber for humans and other organisms on earth, is the net uptake of atmospheric carbon dioxide by plants and is calculated as the difference between GPP and R_A. Heterotrophic respiration, which also releases carbon dioxide back to the atmosphere, depends upon the amount of soil organic matter, the C:N ratio of the soil organic matter, air temperature and soil moisture (Raich *et al.* 1991; McGuire *et al.* 1997; Tian *et al.* 1999). Within an ecosystem, carbon may be stored either in vegetation biomass or in detritus (i.e. litter, standing dead and soil organic matter). In TEM, the carbon in vegetation biomass and detritus are each represented by a single pool. The transfer of carbon between these two pools is represented by litterfall carbon (L_C), which is calculated as a proportion of vegetation carbon. Changes in vegetation carbon (ΔVEGC, also known as biomass increment), detritus (ΔSOILC) and terrestrial carbon (ΔTOTALC) are then determined as a linear combination of these fluxes:

$$\Delta VEGC = GPP - R_A - L_C \quad (6)$$

$$\Delta SOILC = L_C - R_H \quad (7)$$

$$\Delta TOTALC = \Delta VEGC + \Delta SOILC = NPP - R_H = GPP - R_A - R_H \quad (8)$$

Carbon sequestration in undisturbed terrestrial ecosystems can be estimated by the GLS either as the sum of the estimated changes in carbon in vegetation and detritus or by the difference between NPP and R_H (Eq. 8) which is also known as net ecosystem production or NEP.

An important feature of TEM is that the model simulates the influence of terrestrial nitrogen dynamics on terrestrial carbon dynamics. First, the uptake of carbon dioxide by plants is assumed by TEM to be limited by nitrogen availability in most land ecosystems on earth. Tropical forests are the only exceptions, where nitrogen availability is not assumed to limit GPP under contemporary conditions. The effect of nitrogen limitation on GPP is determined by first calculating GPP_C assuming no nitrogen limitation:

$$GPP_C = f(CO_2, ET)\ f(PAR)\ f(CANOPY)\ f(LEAF)\ f(T)\ f(O_3, ET) \quad (9)$$

where CO_2 is atmospheric CO_2 concentration, ET is evapotranspiration, PAR is photosynthetically active radiation, CANOPY is the relative state of a vegetation canopy recovering from a disturbance as compared to the canopy state of a mature, undisturbed stand, LEAF is the monthly leaf area relative to the maximum leaf area of a stand, T is air temperature, and O_3 is atmospheric ozone concentration. The influence of atmospheric CO_2 and O_3 concentrations on GPP depends on the status of vegetation stomates, which close during drier conditions (i.e. low ET) to reduce the uptake of CO_2 or O_3 and open during wetter conditions (i.e. high ET). Details of Equation 9 have been described elsewhere (e.g Raich *et al.* 1991; McGuire *et al.* 1992, 1995, 1997; Pan *et al.* 1998; Tian *et al.* 1999; Felzer *et al.* 2004).

If GPP is limited by nitrogen availability, GPP_N is then calculated based on the effects of nitrogen supply on net primary production (NPP_N):

$$NPP_N = P_{CN}\ (NUPTAKE + NMOBIL) \quad (10)$$

$$GPP_N = NPP_N + R_A \quad (11)$$

where P_{CN} is the carbon to nitrogen ratio (C:N) of newly produced plant tissue, NUPTAKE is the amount of inorganic nitrogen acquired by plants from the soil and NMOBIL is the amount of vegetation labile nitrogen mobilized during a particular month (McGuire *et al.* 1997; Pan *et al.* 1998; Tian *et al.* 1999). Similar to GPP_C, NUPTAKE also depends on local environmental conditions (Raich *et al.* 1991; McGuire *et al.* 1992; Felzer *et al.* 2004):

$$NUPTAKE = f(N_{AVL}, H_2O)\ f(CANOPY)\ f(T)\ f(O_3, ET)$$

where N_{AVL} is soil available nitrogen and H_2O is soil moisture. Monthly GPP is then determined as follows:

$$GPP = min\ (GPP_C, GPP_N) \quad (12)$$

In TEM, the uptake of atmospheric CO_2 by plants is assumed to follow Michaelis-Menten kinetics such that the effect

of atmospheric CO_2 at time t as modified by ET on the assimilation of CO_2 by plants is parameterized as follows:

$$f(CO_2(t)) = (C_{max}\ CO_2(t)) \ / \ (kc + CO_2(t)) \quad (13)$$

where C_{max} is the maximum rate of C assimilation, and kc is the CO_2 concentration at which C assimilation proceeds at one-half of its maximum rate (i.e., C_{max}). Because the response of carbon uptake by plants to atmospheric CO_2 concentrations is uncertain (Sokolov *et al.* 2009), we examine the influence of this uncertainty on terrestrial carbon dymanics by adjusting the value of kc in our uncertainty analyses.

The Natural Emissions Model (NEM) has been embedded within the TEM infrastructure as described in Schlosser *et al.* (2007). As such, the CH_4 and N_2O flux estimates by NEM are directly based on monthly TEM estimates of soil organic carbon. Although the simulated carbon and nitrogen dynamics of NEM are still mostly separated from those in TEM, the embedded NEM provides a platform for improving the linkages between the two biogeochemistry-models. For example, NEM estimates of CH_4 emissions diminish the stock of soil organic carbon estimated by TEM. The embedded NEM allows simulation of daily CH_4 and N_2O emissions based on monthly estimates of soil organic carbon by TEM combined with the CLM estimates of daily soil temperatures, daily and hourly soil moistures, hourly rainfall intensities and storm durations. CLM also provides all data on soil properties required by TEM/NEM. Fluxes of CO_2, CH_4 and N_2O are passed to atmospheric model and are used in calculations of the corresponding gases by the atmospheric chemistry sub-model.

3. Model Evaluation

As mentioned earlier, the MESM can be run either in concentration-driven or emissions-driven mode. In historical simulations, the MESM is forced by the prescribed changes in by greenhouse gases and ozone concentrations, aerosols, and solar irradiance. Greenhouse gas concentrations and stratospheric aerosols from volcanic eruptions are taken from the NASA GISS modeling group forcing suite. Miller *et al.* (2014) describe the methods for updating the greenhouse gas concentrations from Hansen *et al.* (2007) and the volcanic aerosol optical depths from Sato *et al.* (1993). Sulfate aerosol loadings are from Smith *et al.* (2011) extended by Klimont *et al.* (2013), solar irradiance is from the Kopp and Lean (2011) dataset, and ozone concentrations are from the SPARC dataset used in the CMIP5 experiments (Cionni *et al.*, 2011). In future climate simulations, the MESM is driven by anthropogenic emissions of different gases produced by the MIT Economic Projection and Policy Analysis (EPPA) model (Paltsev *et al.*, 2005).

3.1 Distribution of climate parameters and characteristics describing model response to external forcing.

To determine climate model parameters that produce changes in surface air and ocean temperatures consistent with available observations, 1800 historical simulations from 1861 to 2010 were carried out changing climate sensitivity, the rate of ocean heat uptake and the strength of aerosol forcing over wide ranges. Probability distributions for climate parameters were constructed using the methodology described in Forest *et al.*, (2002 and 2008) and Libardoni and Forest (2011 and 2013). Detailed descriptions of the distributions obtained using different observational data sets, different estimates of natural variability and other assumptions are given in Libardoni *et al* (2017). Below we described our final distributions and present the results of simulations with the set of climate parameters sampled from it. This distribution was derived using multiple datasets for changes in surface temperature from 1905 to 2010 and in ocean heat content from 1990 to 2010. Individual distributions were merged across all surface datasets to produce the final distribution. Estimates of natural variability from all CMIP5 models were used to estimate the noise-covariance matrix.

Table 1 shows medians and 90% probability intervals for model climate parameters from distribution used in this paper. The median values for equilibrium climate sensitivity (ECS, **Figure 2a**) is rather close to the median climate sensitivity of CMIP5 AOGCMs (3.2 K), while the 90% probability interval is shifted toward higher values compared with the CMIP5 models (1.9 to 4.5 K).

To assess uncertainty in the transient climate response (TCR, i.e., temperature change in the time of CO_2 doubling), we carried out a set of climate simulations with a 1% per year increase of CO_2 concentration using 400 samples of climate parameters. To estimate uncertainty in the carbon cycle we calculated carbon uptake by the ocean and terrestrial ecosystems in these simulations. As discussed above, the vertical diffusion coefficient for carbon depends on the vertical diffusion coefficient for heat anomalies. As a result, uncertainty in oceanic carbon uptake is defined by the uncertainty in the heat uptake. In all simulations

Table 1. Percentiles for climate parameters.

	Climate sensitivity	Square root of diffusion coefficient	Radiative forcing due to aerosol radiation interaction
	K	$cm/s^{1/2}$	W/m^2
5%	2.4	0.9	-0.47
50%	3.2	1.8	-0.24
95%	4.6	3.7	-0.05

described in this paper we used K_{vco} =1cm/s and r=0.52 (Eq. 3). Uncertainty in the terrestrial carbon uptake was taken into account by varying the half-saturation constant, kc (Eq. 13). The results of CO_2-enrichment studies suggest that plant growth could increase by 24% - 54% in response to doubled CO_2 given adequate nutrients and water (Raich *et al.* 1991; McGuire *et al.* 1992; Gunderson and Wullschleger 1994; Curtis and Wang 1998; Norby *et al.* 1999, 2005). In the stand-alone TEM, a value of 400 ppmv CO_2 is chosen for the half-saturation constant, kc, so that $f(CO_2(t))$ increases by 37% for a doubling of atmospheric CO_2 (e.g. McGuire *et al.* 1997; Pan *et al.* 1998). A 24% and 54% response to doubled CO_2 would correspond to kc values of 215 and 800 ppmv CO_2, respectively. The sensitivity of plant uptake on CO_2 increase is defined not by the absolute value of $f(CO_2(t))$, which decreases with kc, but by the ratio of $f(CO_2(t))$ to $f(CO_2(0))$ which increases with kc.

Based on a comparison of the TEM version implemented in the MESM with other terrestrial carbon models (Sokolov *et al.*, 2008) and results from stand-alone TEM simulations, different values of kc are used for nitrogen-limited and non-limited ecosystems. In the simulations discussed below, the value of kc was varied from 200 to 800 ppmv CO_2 for nitrogen-limited ecosystems and from 75 to 300 ppmv CO_2 for ecosystems with no nitrogen limitations.

Total carbon uptake can be estimated from available data on carbon emissions and observed CO_2 concentrations and is less uncertain than carbon uptake by the ocean and carbon uptake by terrestrial ecosystem separately. To take this into account, low values of Kv (small carbon uptake by the ocean) are coupled with high values of kc (large terrestrial carbon uptake).

Figure 2b shows frequency distributions for TCR from 400 simulations. The median value for TCR (1.7 K) is close to that for CMIP5 model (1.8 K), while the 90% probability interval (1.4 – 2.0 K) is significantly narrower than estimates based on CMIP5 models (1.2 – 2.4 K). The relatively small range of TCR in our simulations is explained in part by the correlation between climate sensitivity and the rate of oceanic heat uptake imposed by observations (**Figure 3**). Another characteristic often used to describe transient model response to forcing is a "realized warming" defined as a ratio of equilibrium climate sensitivity to TCR. In our simulations, this characteristic ranges from 0.35 to 0.66 (90% interval) with median value of 0.54. The fact that these values are smaller than corresponding values for CMIP5 model (0.46–0.72 and 0.58) indicates that the rate of oceanic heat uptake in CMIP5 models is most likely smaller than in our simulations.

The transient climate response to cumulative carbon emission (TCRE), is defined as the ratio of surface warming to cumulative implied carbon emissions at the time of CO_2 doubling from simulations with a 1% per year increase in CO_2 concentrations (Matthews *et al.* 2009). Values of TCRE in MESM simulations vary (90% range) from 1.2 to 1.9 K/EgC (**Figure 2c**). According to Gillett *et al.*, (2013), a similar range for CMIP5 models is 0.8–2.4 K/EgC. At the same time observationally constrained range, obtained using CMIP5 simulations and observed temperature to 2010 is 0.7–2.0 K/EgC (Gillett *et al.*, 2013).

To evaluate uncertainty in long-term climate system response implied by the distribution of climate parameters described above, we carried out an ensemble of simulations using RCP8.5 GHGs concentrations. Comparison between the results from this ensemble and those from the multi-model CMIP5 ensemble are presented in **Table 2**. The MESM simulates less surface warming during the 21st century than the CMIP5 ensemble which, in part, may be explained by the fact that most of CMIP5 models overestimate warming in the first decade of 21st century.

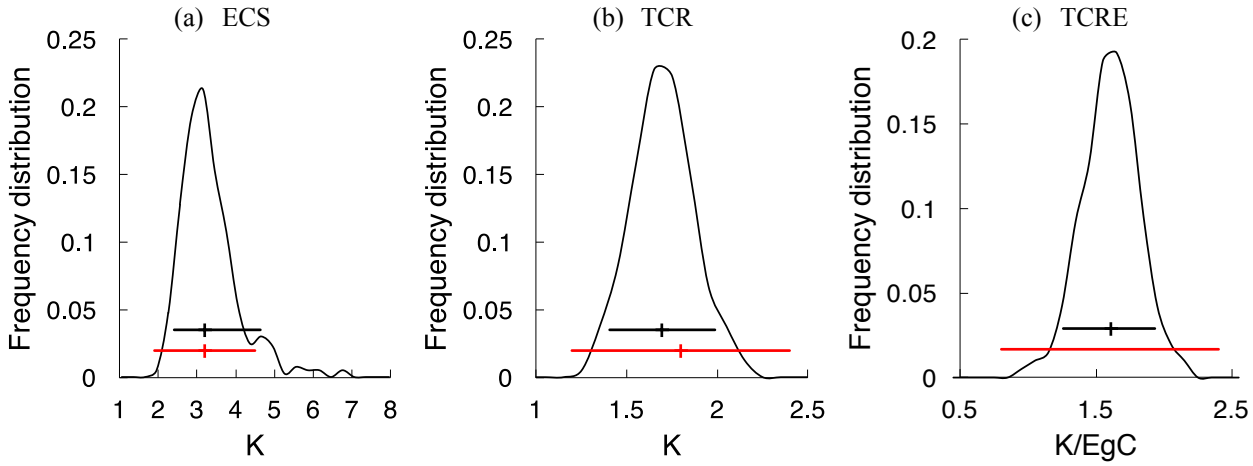

Figure 2. Frequency distribution of (a) ECS, (b) TCR and (b) TCRE. Vertical line shows median value and horizontal bar shows 90% probability interval. Red line CMIP5 estimate, from Table 9.5 of IPCC (2013) for TCR and from Gillett *et al.*, (2013) for TCRE.

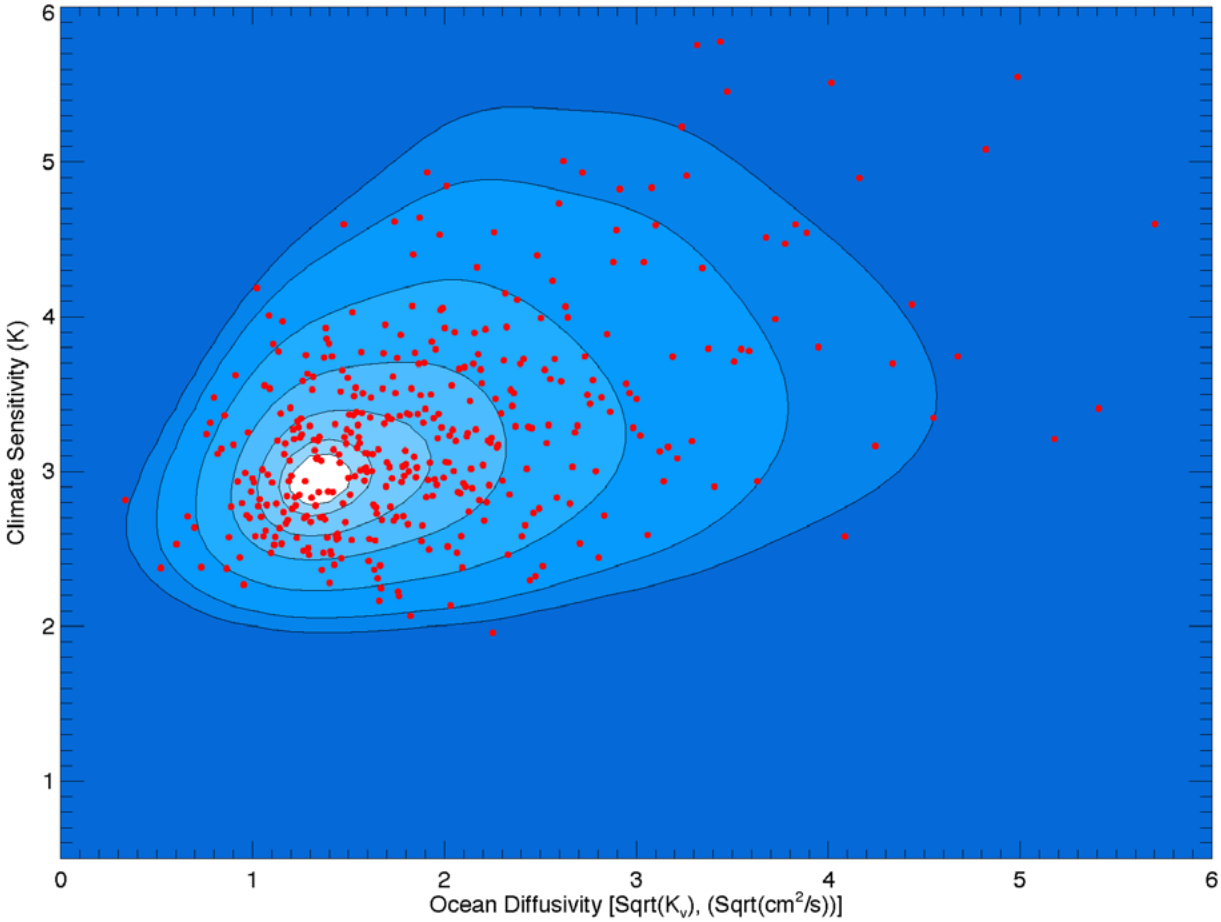

Figure 3. Distribution of climate sensitivity and the rate of ocean heat uptake (square root of vertical diffusion coefficient). Red dots show values of CS and SQRT(Kv) for 400 samples.

The contour lines are for the 5,10,25,50,75,90 and 95% percentiles.

At the same time, MESM simulates stronger temperature increase during 22nd and 23rd centuries than CMIP5 models. It should be kept in mind that from the 39 CMIP5 models that ran the RCP8.5 simulation only 12 were run beyond 2100. As can be seen on Figure 12.5 of IPCC (2013), the multi-model mean surface warming in 2100 is smaller for these 12 models than for all 39 models. The use of a different number of CMPI5 models in different simulations somewhat complicates the comparison between CMIP5 and MESM results. The estimates for ECS and TCR, shown above, are from simulations with 23 and 30 CMIP5 models, respectively (Table 9.5 in IPCC 2013). The TCRE estimates are based on the results of 15 CMIP5 ESMs (Gillett *et al.*, 2013).

3.2 Historical Climate Change

To assess the quality of the probability distributions for climate model parameters, we carried out 400 historical simulations from 1861 to 2010. The model reproduces the observed changes in surface air temperature very well (**Figure 4a**). Temperature averaged over the first decade of the 21st century increases in our simulations relative to the 1861–1880 mean between 0.67 and 1 K (90% probability interval) with a mean value of 0.835 K. Similar to the TCR, the range of temperature change simulated by MESM is significantly narrower than one produced by

Table 2. Median values and 90% probability intervals for surface air temperature anomaly relative to 1986-2005 mean in simulations with RCP8.5 scenario. CMIP5 results are from Table 12.2 of IPCC (2013).

	CMIP5		MESM	
2046–2065	2.0	(1.4, 2.6)	1.7	(1.3, 2.0)
2081–2100	3.7	(2.6, 4.8)	3.1	(2.6, 3.8)
2181–2200	6.5	(3.3, 9.8)	7.0	(5.7, 8.9)
2281–2300	7.8	(3.0, 12.6)	8.9	(6.9, 11.0)

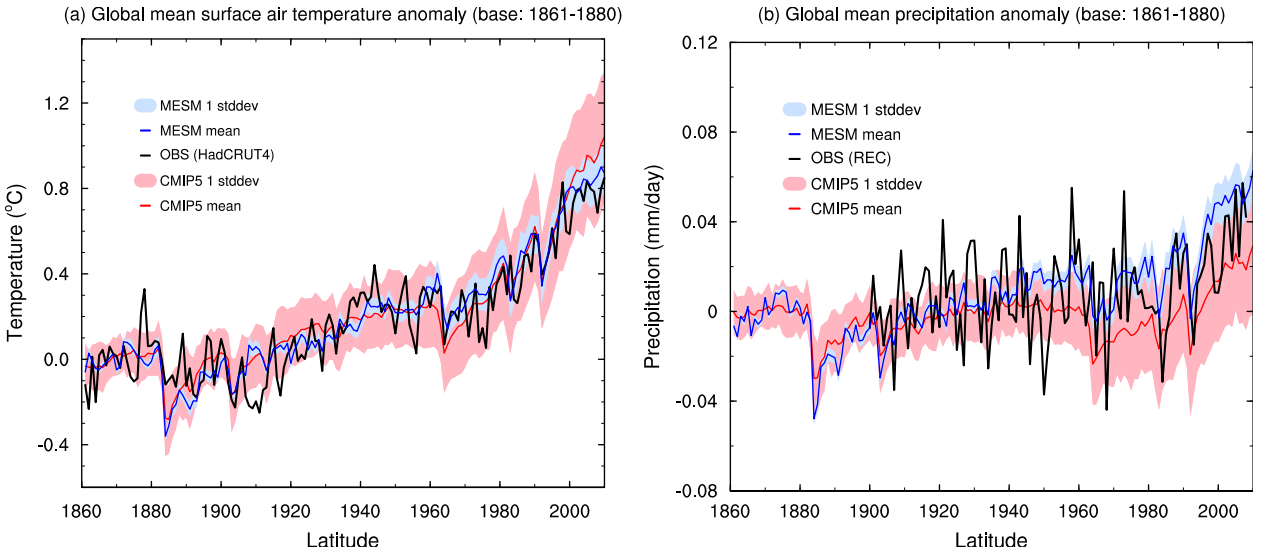

Figure 4. Time series of global mean surface air temperature and precipitation relative to 1861–1880 mean. The simulations with the MESM are shown in blue (ensemble mean and one standard deviation in shading) and the simulations from the CMIP5 multi-model ensemble are shown in red (multi-model ensemble mean and one standard deviation in shading). After 2006, simulations under the RCP8.5 are used. Observations are shown in black lines, namely the HadCRUT4 (Morice *et al.*, 2012) and global reconstructed precipitation (REC) data (Smith *et al.*, 2012) for temperature and precipitation respectively.

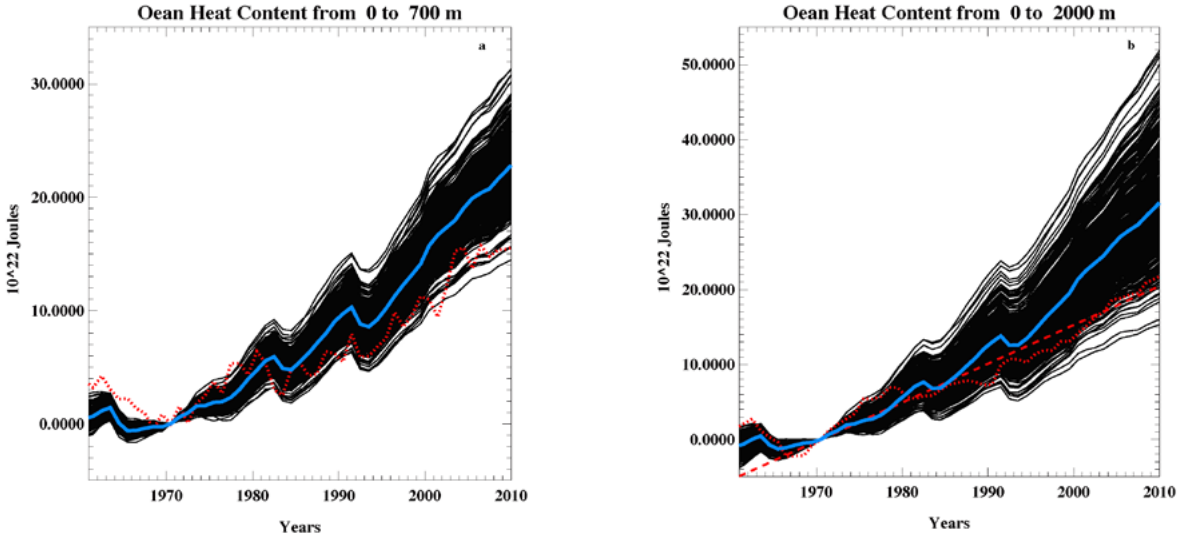

Figure 5. Changes in ocean heat content relative to 1971 in the top 700m (a) and top 2000 m (b). Black lines are ensemble of MESM simulations. Blue lines are ensemble means. Red lines are observations from Levitus *et al.* (2012).

CMIP5 models. The MESM ensemble mean agrees better with the observation than the CMIP5 mean, especially after year 2000, when CMIP5 models overestimate observed warming. Changes in global mean precipitation simulated by MESM (**Figure 4b**) also agree well with observations, especially the increase in the last 50 years, and improves upon the simulations by the CMIP5 models. However, inter-annual variability simulated by MESM is much smaller than observed. The MESM simulates a larger increase in the ocean heat content both in the top 700m and 2000m (**Figure 5**) compared with observations and CMIP5 models (Figure 9.17 in IPCC 2013). At the same time, sea level increases due to thermal expansion at the rate of 0.85 (0.625–1.4) mm/yr between 1971 and 2010 and at the rate of 1.2 (0.96–1.6) mm/yr between 1993 and 2010. These trends are not too different from the estimates given by IPCC 2013: 0.8(0.5 to1.1) mm/yr and 1.1(0.8 to 1.4) mm/yr, respectively (Table 3.1 in IPCC 2013).

While the TEM calculates carbon fluxes for natural ecosystems using potential land cover distribution, CO_2 emissions associated with agricultural activity are provided by the

EPPA model in the emissions-driven simulations. Nonetheless, terrestrial carbon uptake estimates generally fall within the range of the Global Carbon Project multi-model analysis (Le Quéré *et al.*, 2016), while being smaller than the Global Carbon Project's estimate obtained as the residual from the global carbon budget (**Figure 6a**). The median value of the terrestrial carbon uptake averaged over 2000–2009 (**Figure 7a**) is about 0.25 GtC/y smaller than the best estimate provided by IPCC (2013). This can be partially attributed to the fact that nitrogen deposition is not taken into account. Simulated uncertainties in terrestrial uptake are also smaller than those suggested by IPCC (2013). Ensemble mean carbon uptake by the ocean (**Figure 6b**) agrees very well with data from the Global Carbon Project (Le Quéré *et al.*, 2016). However, the range on oceanic carbon obtained in our simulations is slightly shifted towards high values compare to IPCC estimate (**Figure 7b**).

3.3 Present-day Climate

3.3.1 Meteorological Variables

In this section, we compare annual mean data from our simulations averaged over 1991–2010 period with available observations and results from CMIP5 (Taylor *et al.*, 2011) simulations. While simulating changes in global mean temperature and precipitation really well (Figure 4), the MESM simulations have some difficulties matching observed zonal distributions for present-day climate. MESM simulates somewhat lower temperature in the southern hemisphere and noticeably higher temperature in the mid-latitudes in the northern hemisphere (**Figure 8a**). The MESM also overestimates precipitation in the descending branch of mean meridional circulation in the northern hemisphere and underestimate precipitation in the mid-latitude storm track regions (**Figure 8b**), which shows the limitations of using a zonal-mean atmosphere model. The MESM

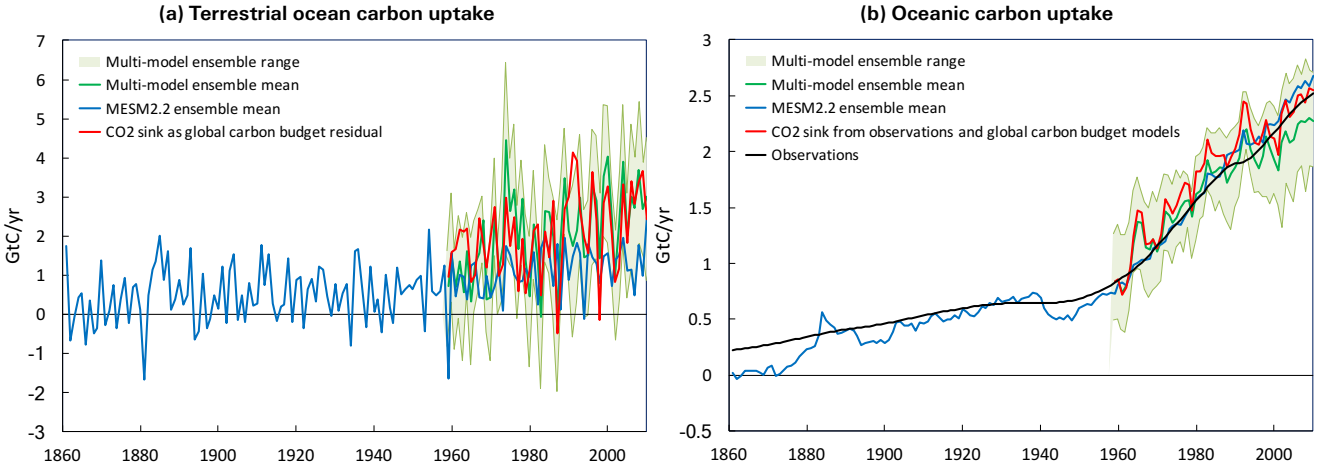

Figure 6. (a) Terrestrial and (b) oceanic carbon uptake. Data for comparison are from Le Quéré *et al* (2016).

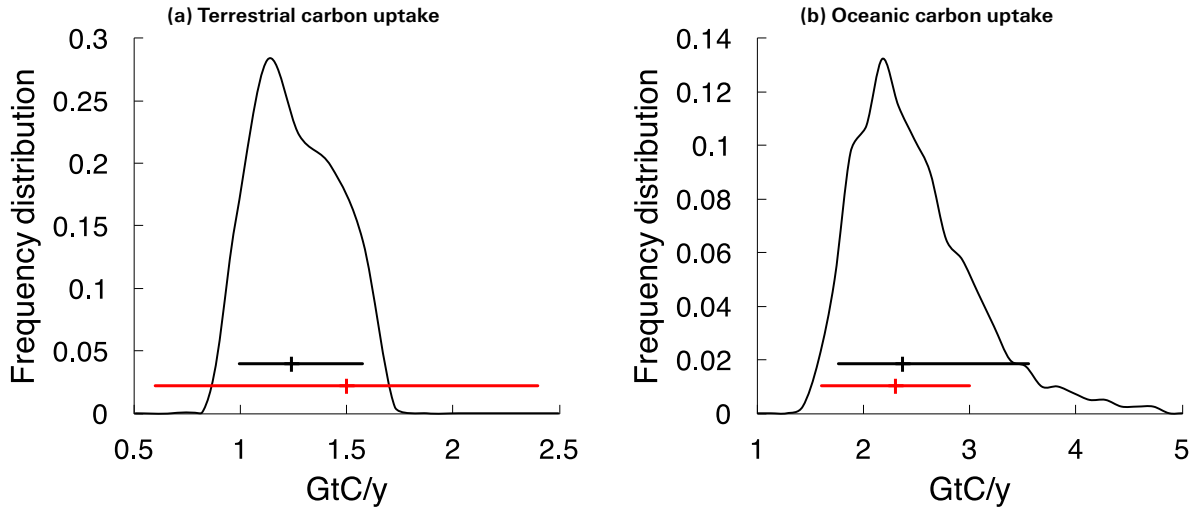

Figure 7. Frequency distribution of (a) terrestrial and (b) oceanic carbon uptake averaged over years 2000–2009. The black line represents the 90% interval from the MESM ensemble. The red line represents the AR5 estimate (Table 6.1 IPCC 2013).

realistically simulates the general characteristics of both surface latent and sensible heat fluxes (**Figure 8c**,**d**) and their latitudinal distributions fit within the range of the CMIP5 state-of-the-art climate except over a few latitude bands, specifically 20S-Equator and 20N-35N for latent heat flux and 90S-80S and 65–75N for sensible heat flux. Latitude-height cross sections of annual mean temperature, specific humidity and relative humidity are shown in **Figure 9**. The MESM is able to reproduce the overall latitudinal and vertical distributions of temperature and humidity generally well despite a cold bias in the polar regions, the maximum specific humidity in the equatorial regions not extending into the upper troposphere and high relative humidity values, especially in the mid-latitudes and polar regions.

3.3.2 Terrestrial Water Cycles

Global precipitation over land constitutes a substantial segment of the terrestrial water cycle and strongly influences the carbon and nutrient cycles tracked by TEM. As such, we compared MESM to the observationally-based estimate from the Global Precipitation Climatology Project

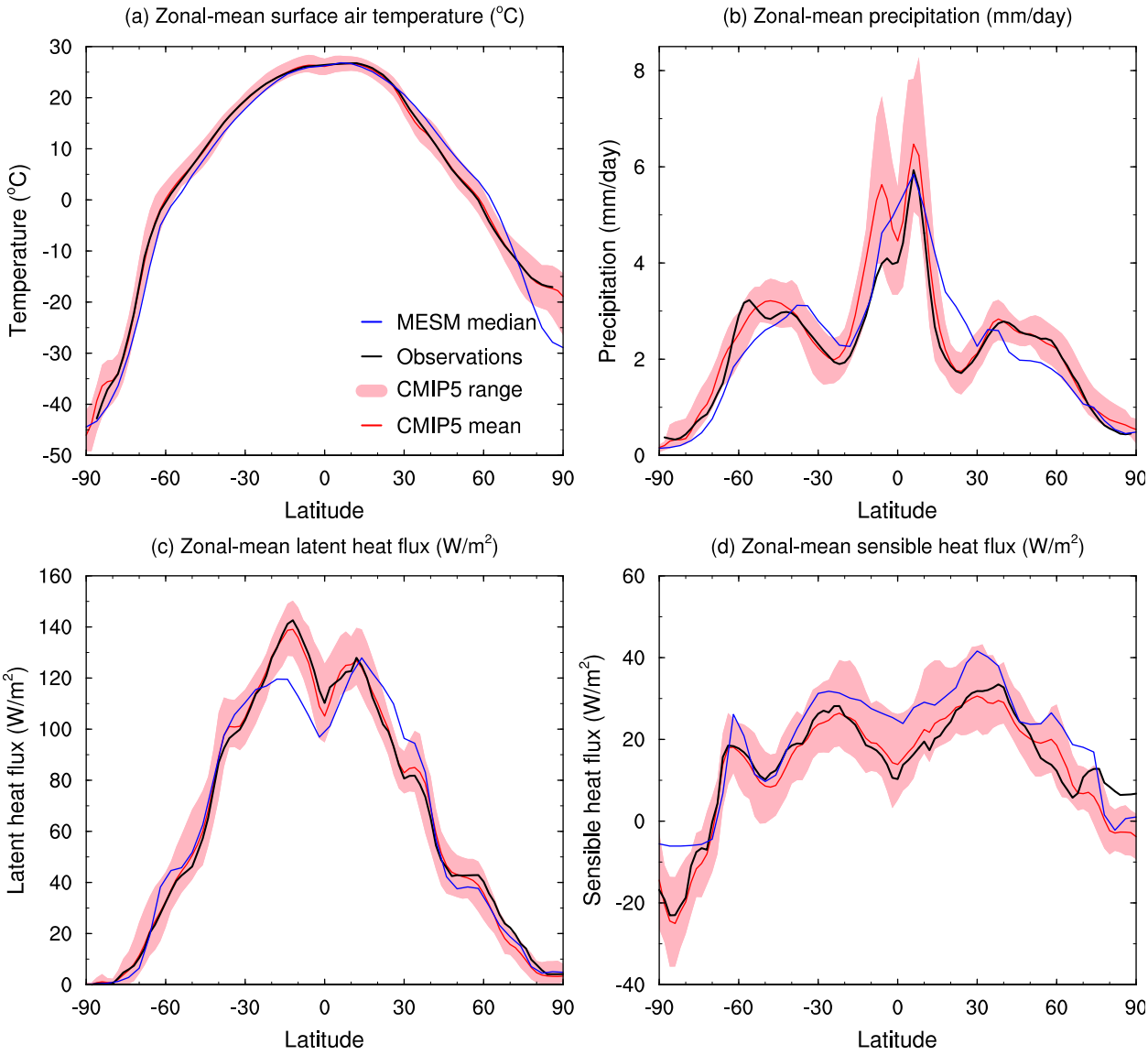

Figure 8. Zonal distribution of (a) surface air temperature (in ºC), (b) precipitation (in mm/day), (c) surface latent heat flux (in W/m^2), and (d) surface sensible heat flux (W/m^2) averaged over the 1991–2010 period. The MESM simulation with the median values of climate parameters (climate sensitivity, ocean heat uptake rate and net aerosol forcing) is shown in blue. Simulations from the CMIP5 multi-model ensemble are shown in red (multi-model ensemble mean and full range in shading). After 2006, simulations under the RCP8.5 are used. Observations are shown in black lines, namely the HadCRUT4 (Morice *et al.*, 2012), GPCP v2.3 (Adler *et al.* 2003) and MERRA2 (Gelaro *et al.*, 2017) for temperature, precipitation and the heat fluxes respectively.

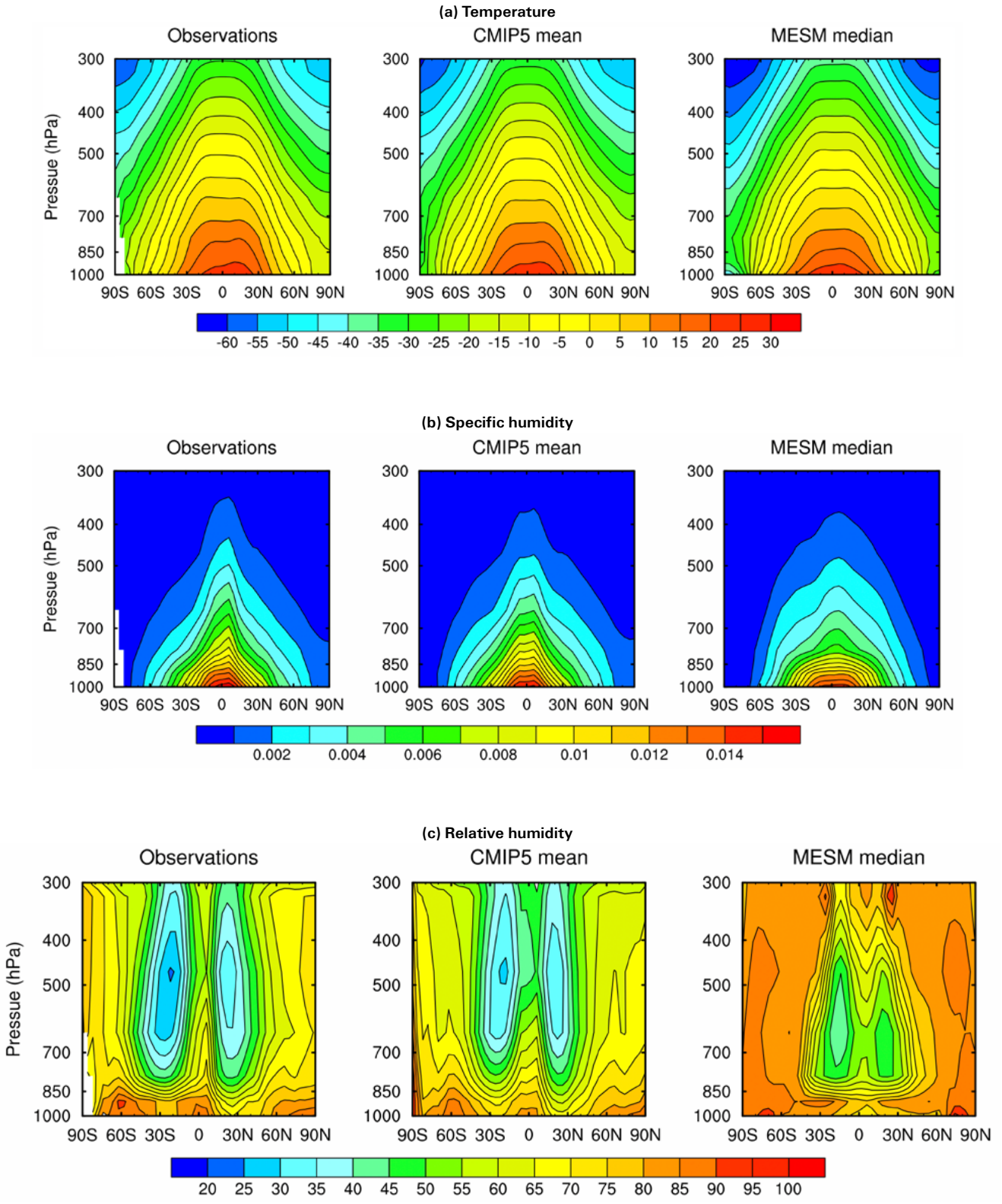

Figure 9. Latitude-height cross section of (a) temperature (in ºC), (b) specific humidity (in kg/kg), and (c) relative humidity (in %) averaged over the 1991-2010 period. Observations from MERRA2 (Gelaro *et al.*, 2017) are shown on the left panels, the CMIP5 multi-model ensemble mean is shown in the middle panels and the MESM simulation with the median values of climate parameters (climate sensitivity, ocean heat uptake rate and net aerosol forcing) is shown in the right panels. After 2006, CMIP5 simulations under the RCP8.5 are used.

(GPCP, Adler *et al.* 2003 and Adler *et al.*, 2012). We find that the MESM estimate of land-only precipitation depicts the key seasonal and zonal attributes to a level that is very comparable with the CMIP5 models (**Figure 10**). At the global scale (**Table 3**), the MESM is closely aligned with the GPCP estimate and also is centrally placed across the estimates of the CMIP5 models (equally biased high and low across each of these climate models). Some notable discrepancies are that land-only precipitation is biased low during the NH summertime midlatitude regions. This deficiency in summertime precipitation contributes correspondingly to slightly lower evapotranspiration rates compared to most of the CMIP5 models (**Figure 11** and Table 3), although MESM is still within the range of CMIP models. For total runoff, MESM produces more runoff on the global scale than the CMIP5 models (Table 3), although the predominant seasonal and latitudinal features are preserved (**Figure 12**). As previously discussed in Section 2.4, the modification of the soil-infiltration scheme (i.e. removal of enhanced hydraulic conductivity under excessive dry soil conditions) was of considerable benefit to the performance of evapotranspiration and runoff rates shown here.

3.3.3 Ecosystem Productivity and Natural Emissions of Trace Gases

Net Ecosystem Productivity: The results from the key water and energy fluxes of the land system provide a first-order expectation to the climatological behavior of the terrestrial carbon cycle within MESM. As in previous evaluations of the land systems implemented within this Earth-system model framework (Schlosser *et al.*, 2007), we focus on the net exchange of carbon between the land and the atmosphere, which represents a key coupling. Further, the TEM model is commonly used in a "standalone" configuration to simulate historical conditions and thus driven by observed atmospheric conditions (e.g. Zhu *et al.*, 2011), and previous evaluations have used this as a baseline for TEM reduced-form configuration with the MESM framework (e.g. Schlosser *et al.*, 2007). We extend this approach by considering the net ecosystem productivity (NEP) of TEM on a month versus latitude projection (**Figure 13**). We find

Table 3. Summary statistics for simulated fluxes in the land water/energy cycles. Shown are correlations and bias (in mm/day) of precipitation, evapotranspiration, and runoff. The correlations are performed on the month vs. latitude projections shown and discussed. For precipitation, all model simulations are judged against the Global Precipitation Climatology Project (GPCP) observations. For evaporation and runoff, these metrics are performed for the CMIP5 models against the MESM result in order to convey the degree of consistency between the more complex CMIP models to MESM's intermediate complexity. Note that for the ACCESS1-3 outputs of total runoff were not made publicly available (N/A). Sign convention for bias is positive when CMIP5 value exceeds MESM or model exceeds observation.

	Evaluation with GPCP Observed Precipitation (1981-2005)		Comparison to MESM Simulation (1981-2005)			
Model	Correlation	Bias	Evaporation		Runoff	
			Correlation	Bias	Correlation	Bias
MESM	0.91	-0.04				
ACCESS1-3	0.95	0.48	0.85	0.69		N/A
CanESM2	0.94	-0.50	0.90	-0.02	0.62	-0.43
CCSM4	0.95	0.32	0.90	0.69	0.72	-0.19
CNRM-CM5-2	0.93	0.10	0.90	0.50	0.58	-0.14
CSIRO-Mk3-6-0	0.91	-0.27	0.86	0.01	0.70	-0.24
FGOALS-g2	0.94	0.07	0.87	0.49	0.73	-0.07
GFDL-ESM	0.96	0.32	0.90	0.61	0.77	-0.15
GISS-E2-H	0.89	0.47	0.83	0.73	0.66	-0.35
HadGEM2/CM3	0.93	0.01	0.85	0.48	0.57	-0.21
IPSL-CM5A-MR	0.90	-0.29	0.84	0.27	0.67	-0.19
MIROC5	0.95	0.54	0.86	0.73	0.72	-0.07
MPI-ESM-MR	0.90	-0.25	0.81	0.23	0.50	-0.45
MRI-CGCM3	0.91	0.11	0.83	0.35	0.73	-0.03
NorESM1-ME	0.95	0.20	0.87	0.74	0.70	-0.28

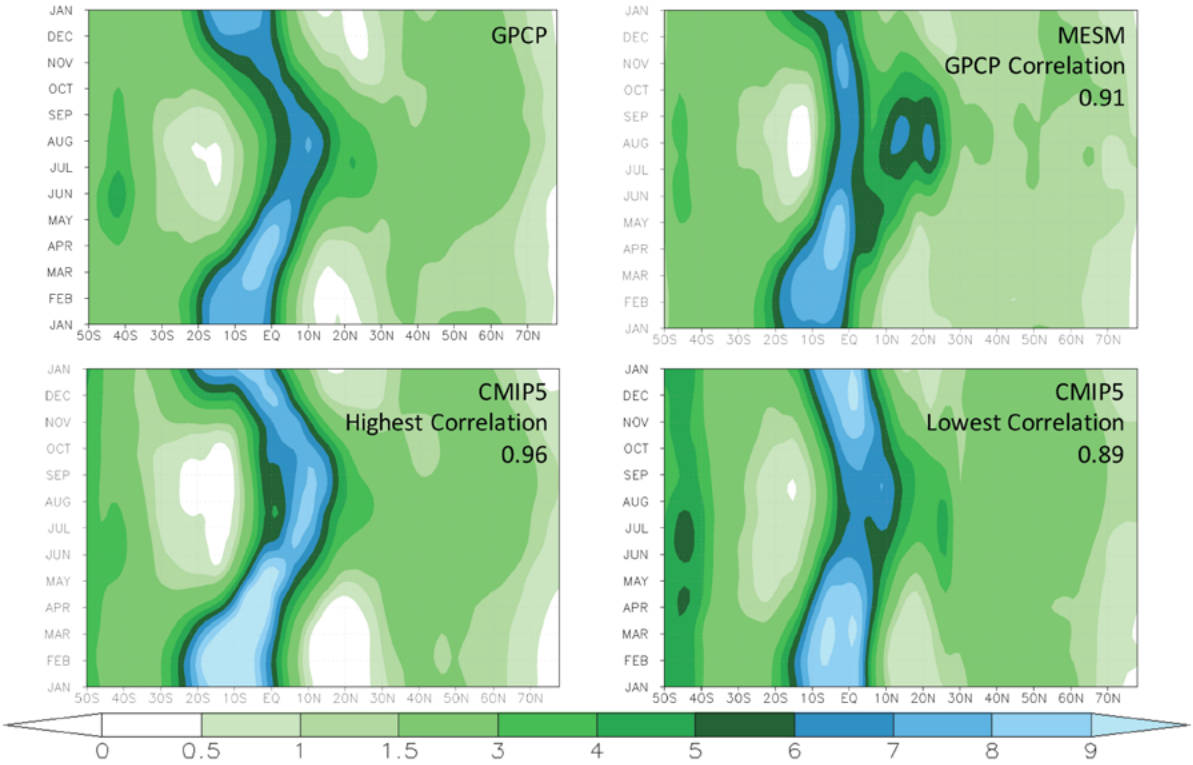

Figure 10. Month vs. latitude profiles of precipitation (mm/day) given by observations from the Global Climatology Precipitation Project (GPCP, upper left); MESM (upper right panel), as well as two simulations from the Coupled Model Intercomparison Project Phase 5 (CMIP5, lower panels). In each of the model-result panels, the correlation of its month vs. latitude profile to that of GPCP is given. The CMIP5 results show the pattern with the highest (lower left) and lowest (lower right) pattern correlation with the GPCP observations.

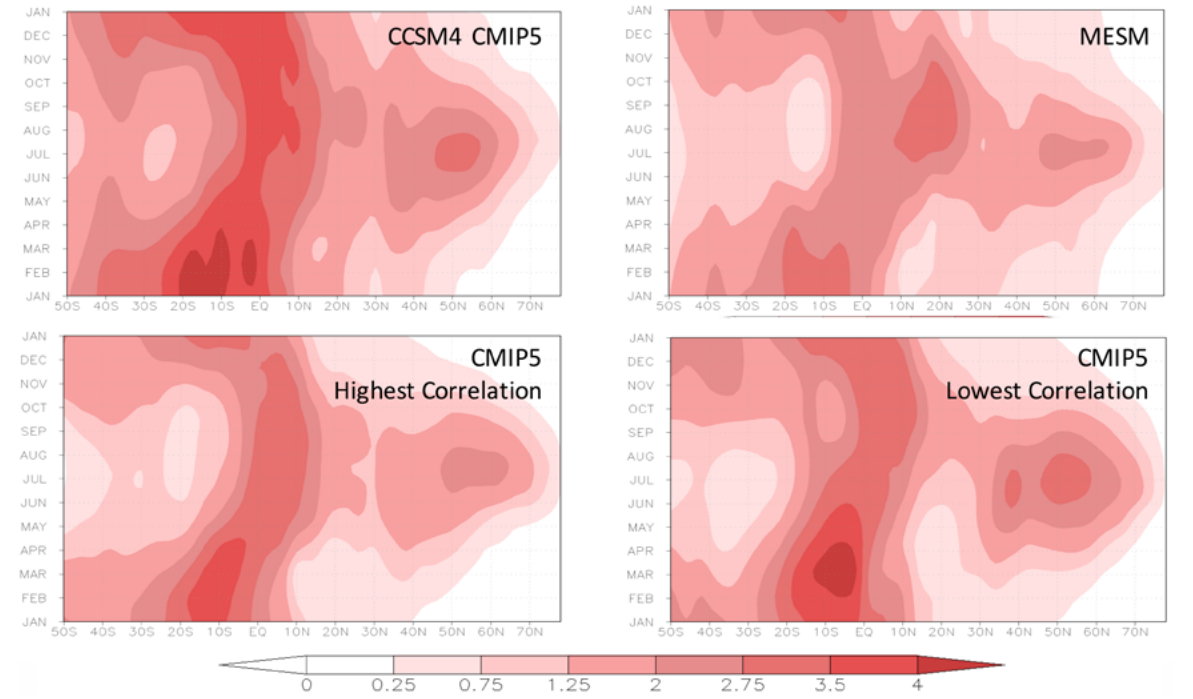

Figure 11. Month vs. latitude profiles of evapotranspiration (mm/day) given by observations from the MESM (upper right panel), as well as two simulations from the Coupled Model Intercomparison Project Phase 5 (CMIP5, lower panels). The CMIP5 results show the pattern with the highest (lower left) and lowest (lower right) pattern correlation with MESM. Also shown is the simulation from CCSM4 (upper left) panel.

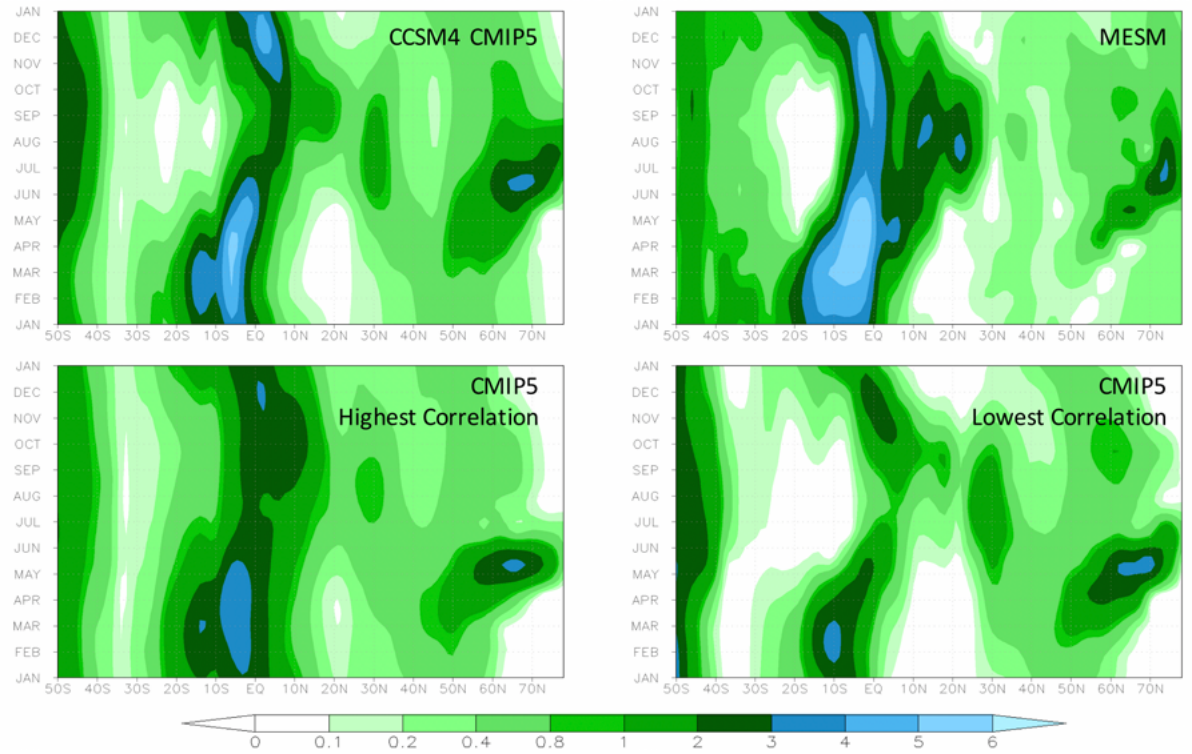

Figure 12. Month vs. latitude profiles of runoff (mm/day) given by observations from the MESM (upper right panel), as well as two simulations from the Coupled Model Intercomparison Project Phase 5 (CMIP5, lower panels). The CMIP5 results show the pattern with the highest (lower left) and lowest (lower right) pattern correlation with MESM. Also shown is the simulation from CCSM4 (upper left) panel.

that the implementation of TEM within the MESM structure preserves all of the salient seasonal and latitudinal attributes as seen in previous evaluations (Figure 19 of Schlosser *et al.*, 2007), and the characteristics of these patterns are consistent and corroborated by recent and detailed simulations with TEM in standalone configuration (e.g. Chen *et al.*, 2011; Zhu and Zhuang, 2013; and Lu *et al.*, 2015). Overall, terrestrial ecosystems represented a net uptake of carbon both globally as well as across all latitudes through our historical period of evaluation (1981–2005). In addition, the strongest (annual) sinks of carbon are found to be across the boreal latitude bands are comprised of extensive forest cover. An additional relative peak is also seen across the southern sub-tropical latitudes and is comparable in magnitude to the sink produced by northern midlatitude ecosystems. Although these areas are strong sinks – they carry a distinct seasonality and serve as considerable carbon sources during the late Fall through early Spring months.

Methane Emissions: In keeping with our overall approach to evaluate the performance of the land biogeochemical fluxes, we have evaluated the methane emissions against previous evaluations with models that contain similar core parameterization recipes but also a recent multi-model assessment (the WETCHIMP study of Melton *et al.*, 2013) with distinct structural differences in overall design as well as implementation of the participating models. In order to provide the most consistent comparative evaluation in this regard, we focus on the historical period of 1993–2004. We find that for nearly all latitudes, the annual emission of methane from MESM falls within the range of the multi-model assessment (**Figure 14**). The most notable exception is found at boreal latitudes with the MESM estimate well above the upper bound of the WETCHIMP range. However, one notable feature of this multi-model assessment is that it did not contain a model participant with TEM as its core ecosystem model that MESM employs. Looking at model-based studies that have used TEM as the core ecosystem model (e.g. Zhuang *et al.*, 2004) as well as an observation-based artificial neural-network method (Zhu *et al.*, 2013) to estimate total methane emissions in boreal latitudes (north of 45˚N), they indicate values on the order of 44 to 54 Tg CH_4/yr. The methane emission rates from the MESM historical simulation provide a more consistent latitude profile of emission across the boreal zone in this regard. Given that the higher boreal emission rates are more closely aligned to the observation-based result, we are confident that the MESM estimate is providing not only a result that is representative of the core ecosystem model behavior (i.e. TEM) but also a value that is empirically defensible.

Nitrous Oxide: In a similar vein to our evaluation of NEP, we find that the MESM historical simulation and a standalone version of CLMCN coupled to a N_2O emissions

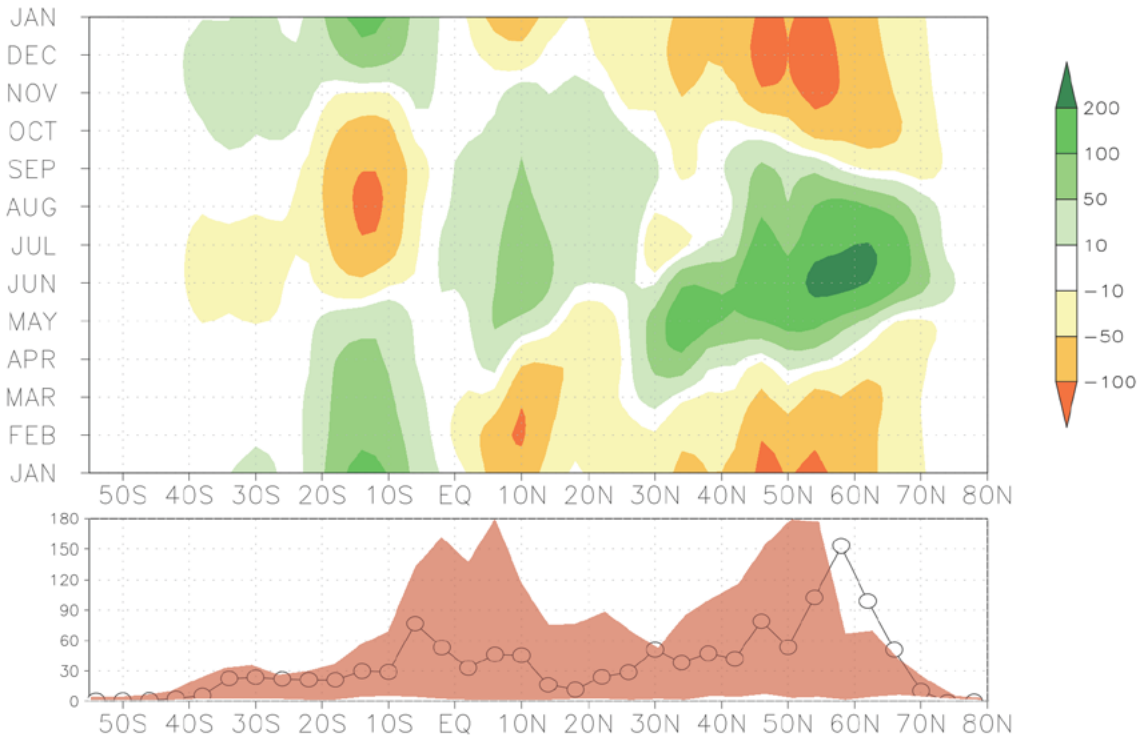

Figure 13. Simulations of emissions of net ecosystem productivity (NEP) by the MIT Earth-System Model (MESM) within the IGSM framework. Top panel displays the month versus latitude results averaged over 1981–2005, and the bottom panel shows the corresponding annual fluxes by latitude. Units are in 109 kg-C/month and 109 kg-C/year, respectively. Shown also in the bottom panel with the shaded red area is the multi-model range from five of the CMIP5 Earth-system models that provided data from historical simulations that cover the evaluation period.

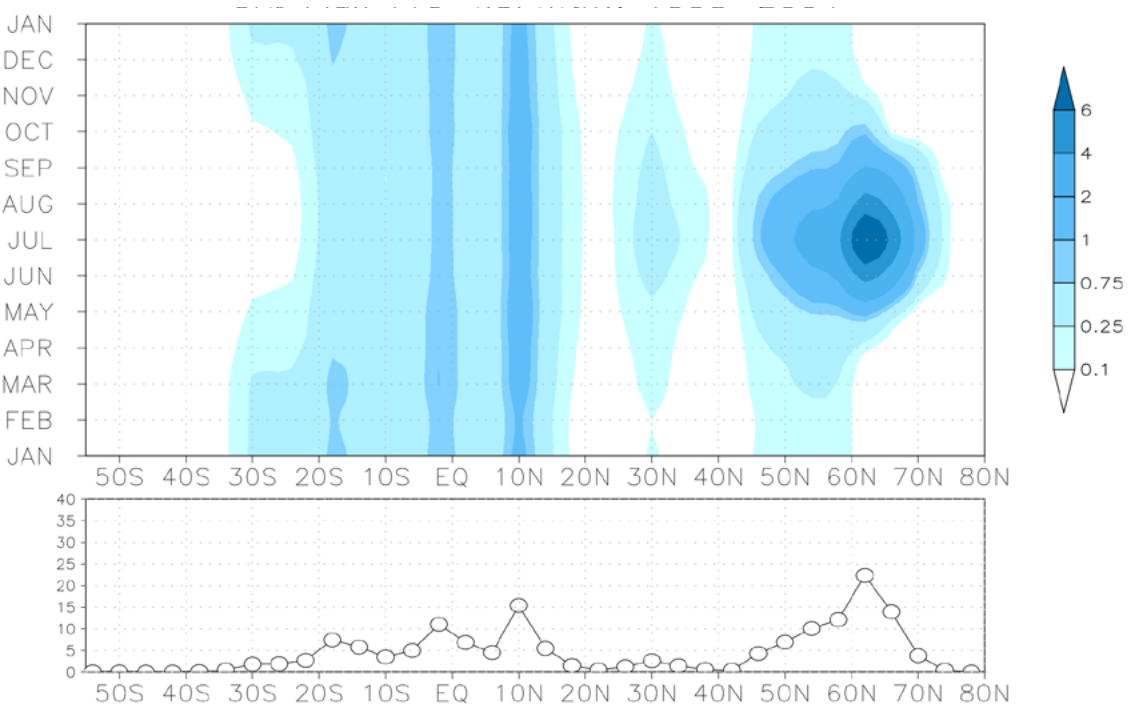

Figure 14. Simulations of emissions of methane by the MIT Earth-System Model (MESM) within the IGSM framework. Top panel displays the month versus latitude results (Units in Tg-CH_4/month) averaged over 1993–2004, and the bottom panel shows the corresponding annual fluxes by latitude (units in Tg-CH_4/year). Shown also in the bottom panel with the shaded red area is the multi-model range from the results of WETCHIMP with. More recent studies (not shown in figure) indicate that the excess in emissions from MESM at high northern latitudes is credible (see corresponding text for details).

model (CLMCN-N2O, Saikawa *et al.*, 2009) share common features but also exhibit distinct differences. It is important, however, to note that this model-to-model comparison cannot provide any judgement on the fidelity or veracity of either model. Rather, this is an evaluation of the sensitivity to the configuration and application of the soil N_2O emissions module (a variant of the DNDC model) within and Earth-system model framework. As such, both of the models exhibit consistent latitudinal locations of relative maximum emission rates (**Figures 15 and 16**) – which occur along the equator as well as during the summer season in both the northern and southern sub-tropical bands. Consistent across all these simulations is that the tropics provide the strongest annual emission source. While both models provide an additional source of emissions across the mid and higher northern latitude bands, a distinct difference is seen in the seasonality of this feature. The CLMCN-N2O model exhibits a distinct summertime peak in emissions that is coincident and widespread across the middle and into higher latitudes. In the MESM zonal configuration – the

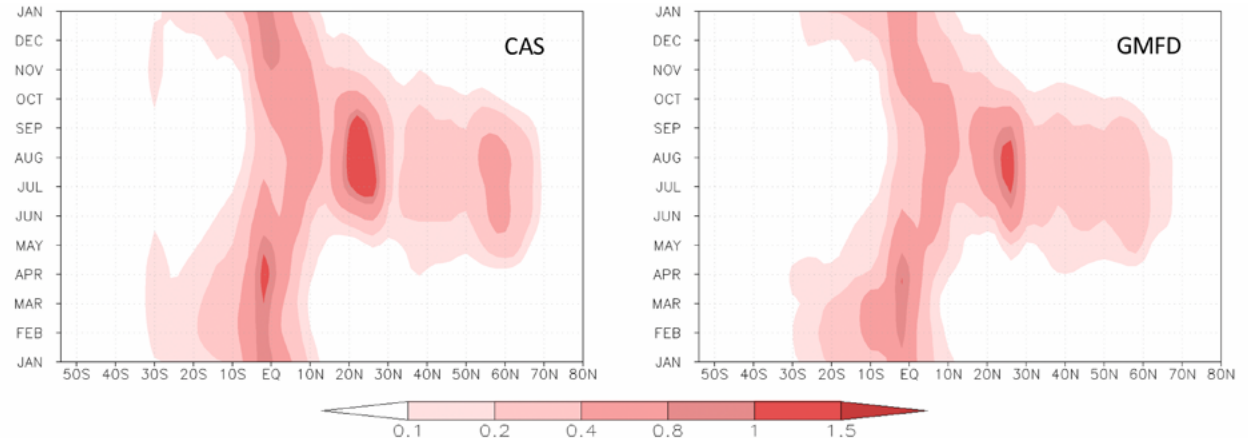

Figure 15. Simulations of soil emissions of nitrous oxide by the CLMCN-N2O model (Saikawa *et al.,* 2013) forced by two different meteorological datasets (CAS and GMFD). Shown are month versus latitude results averaged over 1981–2005. Units are in 108 kg-N_2O/month.

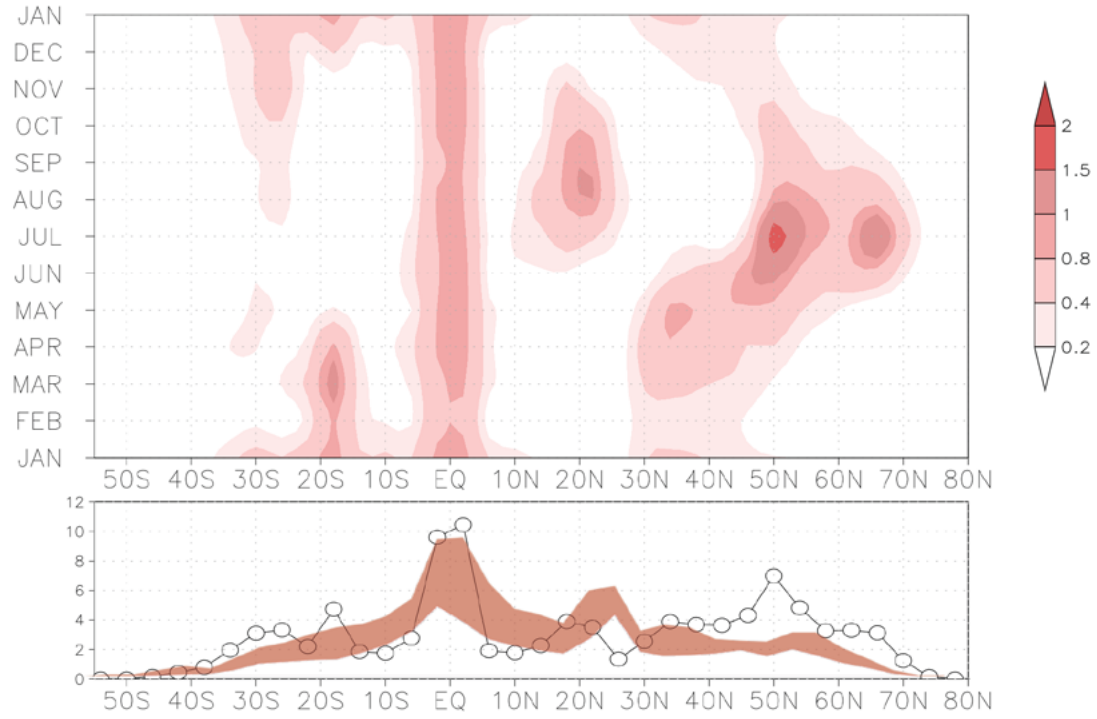

Figure 16. Simulations of soil emissions of nitrous oxide by the MIT Earth-System Model (MESM) within the IGSM framework. The top panel shows month versus latitude results averaged over 1981-2005 with units in 108 kg-N_2O/month. The bottom panel provides the annual emission rates (108 kg-N_2O/year) for the corresponding latitudes of the top panel. Shown also in the bottom panel with the shaded red area is a multi-estimate range based on the results from Saikawa *et al.* (2011) and Hashimoto (2012).

extent and summer timing of the peak is aligned with the CLMCN-N2O estimate between 45–75˚N, however for latitudes 25–45˚N there is an earlier onset and terminus of this feature. Through the course of a number of variants and sensitivity simulations with the IGSM, we have identified that the most likely culprit to this behavior lies within the MESM simulation of land precipitation. When compared to an observationally-based estimate (GPCP), we find that the MESM estimate of precipitation is biased low during the summertime across the corresponding latitude bands (Figure 10). In conjunction with low evapotranspiration rates during the spring (not shown) – soil moisture stores become elevated at these latitudes and trigger the soil anaerobic conditions necessary for denitrification, and thus leads to the earlier emissions peak. However, by the beginning of the summer – elevated evapotranspiration levels combined with a precipitation deficit support dry soils and the emissions processes in MESM become dormant. Nevertheless, we have made salient progress from our earlier implementation (Schlosser *et al.*, 2007) in providing a more consistent depiction of soil N_2O emissions with a reduced form of the model compared to its more detailed counterpart. The scientific community has recently recognized key areas for improvement (Butterbach-Bahl *et al.*, 2013) and will continue to make necessary strides in the detailed modeling of nitrous oxide emissions and verification studies. As such, this strategy will continue to be a critical element of our model development, particularly with regard to the N_2O emissions component.

3.4 Emissions-driven Projections of Future Climate

In the simulations discussed below, the MESM was forced by anthropogenic emissions calculated by the EPPA model, including carbon emissions associated with land use. MESM also takes into account natural emissions of CH_4 and N_2O calculated by NEM.

Wang *et al.*, (1998) describe a tropospheric chemistry and transport scheme for a chemical tracer used in the MESM. In the framework of the Aviation Climate Change Research Initiative (ACCRI, Brasseur *et al.*, 2016), the MESM was used in a tracer transport comparison exercise. In these simulations, the ACCRI 2006 fuel burn inventory (Barret *et al.*, 2010) above 8km were used as a proxy for tracer emissions. Simulations were carried out for six months starting in January and July with tracers being released in the atmosphere during the first month only. Below we show comparisons between results obtained in simulations with the MESM and GEOS-Chem models for three different types of tracers: an inert tracer (no losses), a tropospheric ozone-like tracer with a prescribed a 21-day e-folding lifetime and a tracer with a dry deposition removal process. Results are shown only for simulations started in January because results of simulations started in July look very similar. The total mass of the tracer with dry deposition decreases slightly faster in simulations with MESM than with GEOS-Chem, while the changes for the other two tracers are practically identical in both model simulations (**Figure 17**). **Figure 18** shows latitude- pressure distributions for the ozone-like tracer for the first, third and sixth months of the simulations. Because the total mass of the tracer decreases exponentially, data for the third and sixth months were multiplied by factors of 10 and 10^4, respectively. In general, the study of the impact of aviation emissions on atmospheric chemical composition and climate showed that MESM results lie well within the envelope of the more complex 3-D chemistry-climate models (Olsen *et al.*, 2013).

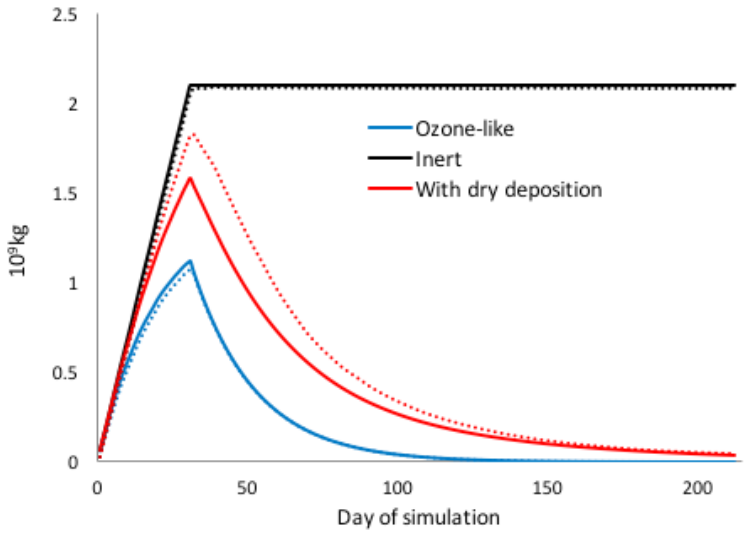

Figure 17. Time evolutions of total mass (10^9 kg) for inert ozone-like and tracer with dry deposition in simulations with January emissions with MIT MESM (solid lines) and GEOS-Chem (dashed lines)

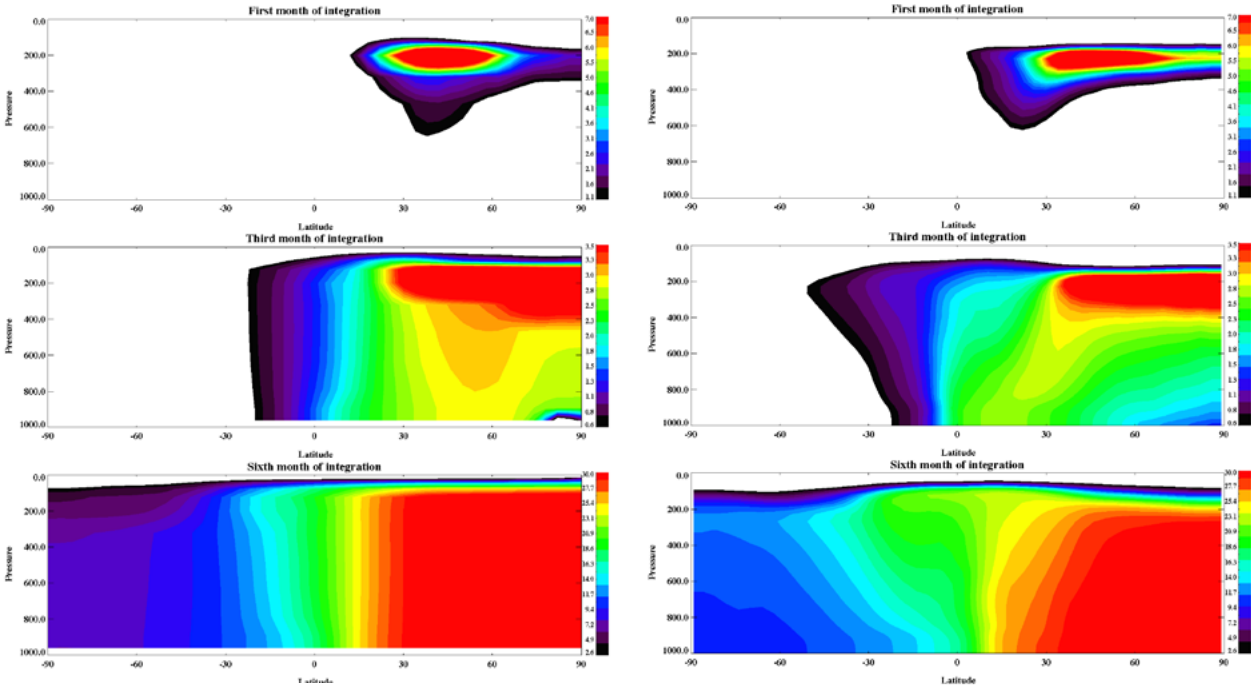

Figure 18. Latitude-pressure distributions of ozone-like tracer concentration (ppbm) in simulations with January emissions for first (top), third (middle) and sixth (bottom) months of simulation. Left column: results obtained with the MIT MESM. Right column: result from GEOS-Chem.

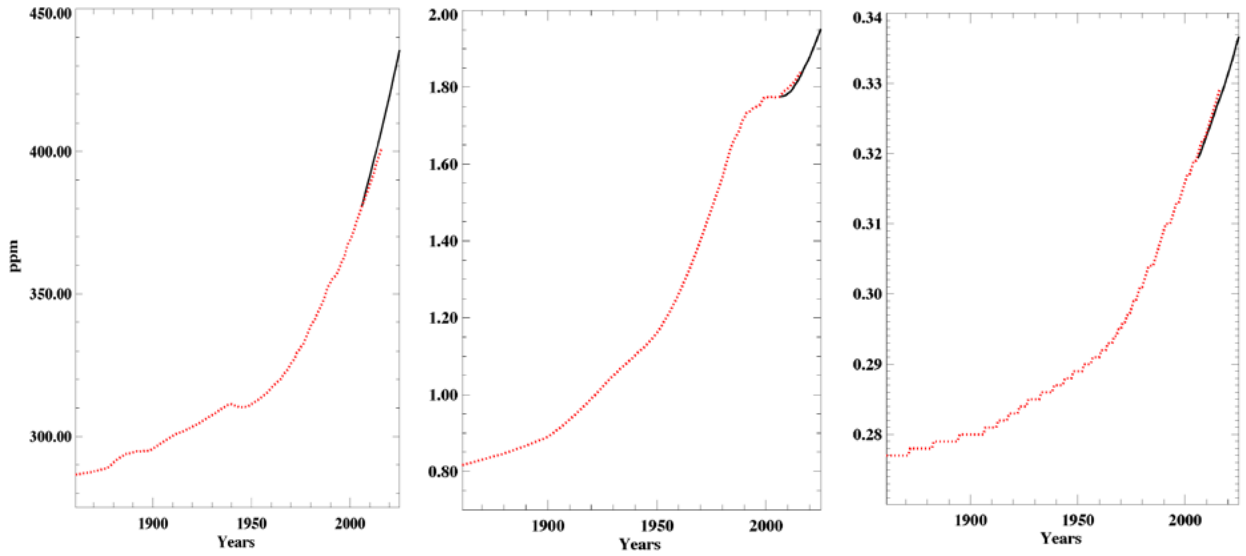

Figure 19. Observed (red) and projected (black) concentrations of CO_2 (left), CH_4 (middle) and N_2O (right).

Our simulations with interactive chemistry start in year 2006 as a continuation of an historical simulation and future projections are then usually given to 2100. Here, however, we will concentrate on short-term simulations (2006–2015) when model mixing ratios using model emissions can be compared with observed mixing ratios.

As can be seen, the MESM simulates global concentrations of the 3 major long-lived greenhouse gases rather well (**Figure 19**). **Figure 20** plots tropospheric mixing ratios for some climate-relevant species (O_3, CH_4, CO, SO_2, NO and NO_2) as well as the very short-lived OH species from the MESM output as well as the zonal average for the ACCMIP archived version of the CESM CAM-Chem, with CAM version 3.5 (available at http://browse.ceda.ac.uk/browse/badc/accmip). The CESM output has 26 vertical levels, which have been regridded to match the 11-level MESM output in Figure 20. In general, the MESM results are comparable to the CESM data, with the vertical and latitudinal distributions

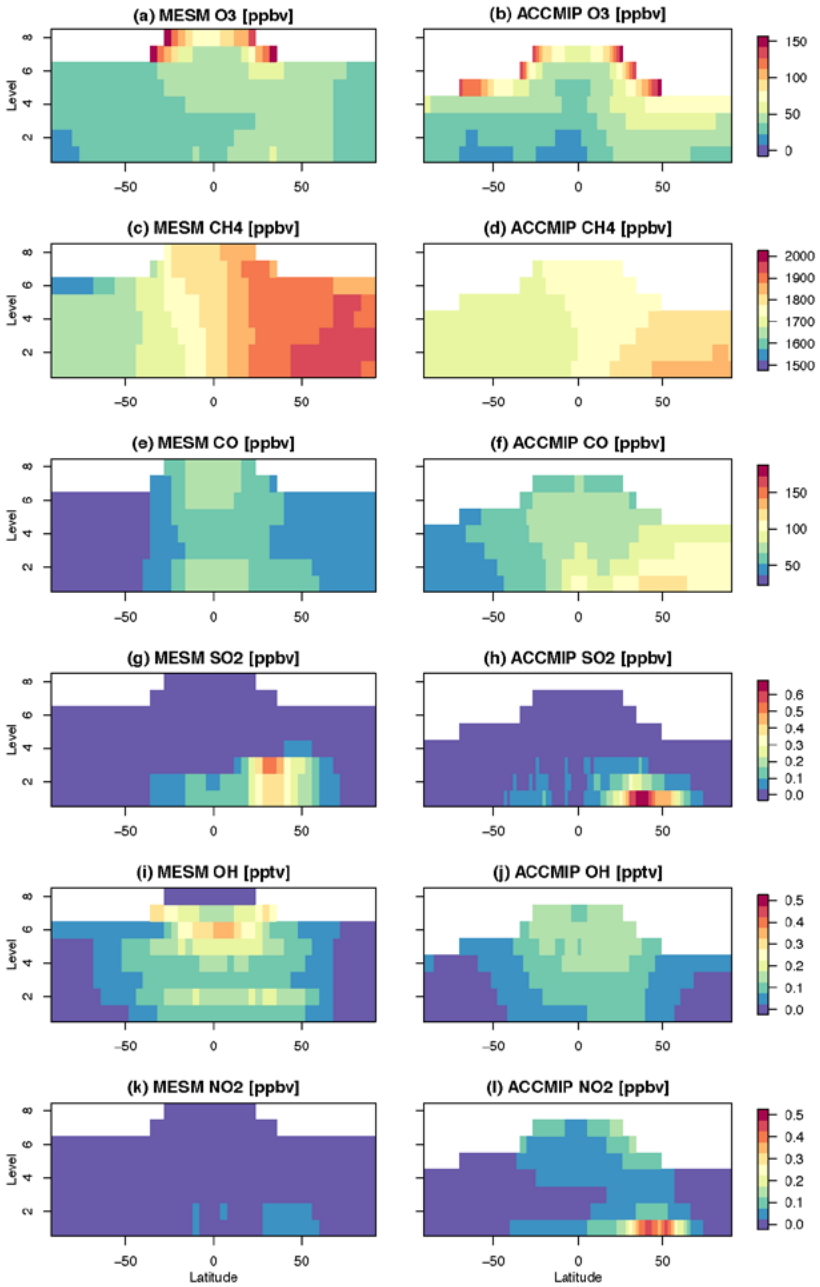

Figure 20. Present-day simulated zonal output from the MESM (left) and zonally averaged output from the CESM CAM-Chem, CAM version 3.5 archived data from the ACCMIP archive (right) for O_3, CH_4, CO, SO_2, OH, and NO_2. The CAM data has been regridded to match the MESM levels, and only data below the tropopause (here defined as 150 ppbv O_3) is shown.

of O_3, CH_4, and OH in fairly close agreement. The MESM does not have the hemispheric asymmetries for CO and NO_2 that are shown in the CESM data, and the MESM vertical distribution of SO_2 peaks at the third level, as a result of SO_2 emissions being distributed evenly in the bottom two layers. In addition, in contrast to most chemistry models (including the CESM-CAM-Chem), MESM does not use prescribed surface concentrations as low boundary conditions.

The radiative forcing and the simulated surface air temperature (not shown) are almost identical in historical (concentration-driven) and emissions-driven simulations. In general, the simulated climates are very similar during the overlapping period of the two simulations (2006–2010).

4. Conclusion

This paper describes the current version of the MIT Earth System Model. The MESM belongs to the class of Earth system models of intermediate complexity (EMICs), which occupy a place between simple conceptual models and comprehensive global circulation models (Claussen *et al.*,

2002). It provides a physical representation of key climate processes and feedbacks, while remaining computationally efficient, and thus allowing for large ensemble of climate simulations to be conduct at significantly less cost than state-of-the-art climate models. The number of climate system components and their complexity are defined by the nature of studies for which the model is intended to be used in. The MESM was designed for and has been used in two major types of studies. First, the MESM has been used to evaluate the uncertainty in key parameters controlling the climate system response to changes in external forcing. Large ensembles of climate simulations are run under historical concentrations of greenhouse gases and aerosols while the relevant climate model parameters are systematically varied (e.g, climate sensitivity, rate of ocean heat uptake, strength of the net aerosol forcing). The simulated climate is then compared with available observations using optimal fingerprint diagnostics to derive probability distributions of the parameters (Forest *et al.*, 2002, 2008; Libardoni and Forest, 2011, 2013). Second, the MESM has been used to investigate the uncertainty in future climate projections arising from the uncertainty in the climate system response to changes in external forcing and the uncertainty in future human activity. This is done by running large ensemble of climate simulations with Latin hypercube sampling of the key climate parameters from their probability distributions under various greenhouse gas and aerosols emissions scenarios developed with the EPPA model (Sokolov *et al.*, 2009; Webster *et al.*, 2012).

Key model requirements to conduct such analysis are: i) the capability to vary key climate model parameters over a wide range representative of our current knowledge of the climate system, ii) computational efficiency in order to run large ensemble for robust uncertainty quantification, and iii) the availability of a comprehensive chemistry model to simulate the fate of various radiatively active chemical species and their impact on the climate system. Since our studies showed that the rate of heat uptake in a 3-dimensional dynamical ocean general circulation model can only be changed over a rather narrow range (Dutkiewicz *et al.*, 2005, Sokolov *et al.*, 2007), the version of MESM used in uncertainty studies incorporates a simplified anomaly-diffusing ocean model, in which the ocean heat uptake rate can be varied over a much wider range. Computational efficiency, required to perform thousands of simulations, is achieved by using a zonally averaged atmospheric model. Nonetheless, the MESM includes a rather comprehensive chemistry model, which can simulate the interaction between different chemical species, such as an impact of changes in NOx emissions on methane lifetime, and the interaction between climate and chemistry, such as an impact of changes in surface ozone concentration on productivity of terrestrial ecosystem (Felzer *et al,* 2004, 2005). As a result, the MESM can be used to evaluate the uncertainty in future climate projections associated with different emission scenarios, accounting for complex interactions and feedbacks between atmospheric chemistry, carbon cycle, and climate.

While not originally designed for such purposes, the MESM has also been used for multi-centennial climate simulations, such as projections beyond 2300 to investigate longer-term commitment and irreversibility (Zickfeld *et al.*, 2013), or preindustrial portions of the last millennium to assess historical carbon-climate feedbacks (Eby *et al.*, 2013). In addition, the MESM has been combined with statistical climate emulator techniques, such as pattern scaling (Schlosser *et al.*, 2013; Monier *et al.*, 2015), to compute regional climate information that not only accounts for the uncertainty in the global climate system response and human activity, but also for the uncertainty in the regional patterns of climate change associated with different climate models. For example, the MESM has been used to derive probabilistic distributions of changes in temperature and precipitation over Northern Eurasia (Monier *et al.*, 2013). Large ensembles of regional climate simulations using the MESM were also used to investigate the risk of permafrost degradation and the associated high latitude methane emissions (Gao *et al.*, 2013), to compute probabilistic projections of water stress over a large portion of Asia (Fant *et al.*, 2016), and to examine the climate change and economic growth prospects for agriculture, road infrastructure and hydropower generation in Malawi (Arndt *et al.*, 2014).

Overall, the results presented in the paper show that, despite simplifications made in the model, the MESM simulates rather well changes in observed climate since the middle of 19th century as well as the main features of present-day climate. The results of the simulations performed in emissions-driven model also compare favorably with results obtained with comprehensive climate-chemistry models and available observations. Therefore, the MESM provide a valuable and efficient tool for climate change modeling, uncertainty quantification and climate risk analysis.

Acknowledgments

This work was supported by **U.S. Department of Energy (DOE)**, Office of Science under DE-FG02-94ER61937 and other government, industry and foundation sponsors of the MIT Joint Program on the Science and Policy of Global Change. For a complete list of sponsors and U.S. government funding sources, see http://globalchange.mit.edu/sponsors. Data presented in the paper are available at http://hdl.handle.net/1721.1/113339.

5. References

Adler, R.F., G.J. Huffman, A. Chang, R. Ferraro, P. Xie, J. Janowiak, B. Rudolf, U. Schneider, S. Curtis, D. Bolvin, A. Gruber, J. Susskind, P. Arkin and E. Nelkin (2003): The version 2 Global Precipitation Climatology Project (GPCP) monthly precipitation analysis (1979–present). *J Hydrometeor* **4**(6): 1147–1167

Adler, R.F., G. Gu and G. Huffman (2012): Estimating Climatological Bias Errors for the Global Precipitation Climatology Project (GPCP). *J Appl Meteorol Climatol* **51**, 84–99

Andrews T., J.M. Gregory, M.J. Webb and K.E. Taylor (2013): Forcing, feedbacks and climate sensitivity in CMIP5 coupled atmosphere-ocean climate models. *Geophys Res Lett* **39**, L09712

Andronova, N.G. and M.E. Schlesinger (2001): Objective estimation of the probability density function for climate sensitivity. *J Geophys Res* **106**(D19): 22,605–22,612

Arndt, C., A. Schlosser, K. Strzepek and J. Thurlow (2014): Climate change and economic growth prospects for Malawi: An uncertainty approach. *Journal of African Economies* **23**, ii83-ii107

Balesdent, J., C. Chenu and M. Balabane (2000): Relationship of soil organic matter dynamics to physical protection and tillage. *Soil and Tillage Research* **53**, 215–230

Barrett, S., M. Prather, J. Penner, H. Selkirk, S. Balasubramanian, A. Dopelheuer, G. Fleming, M. Gupta, R. Halthore, J. Hileman, M. Jacobson, S. Kuhn, S. Lukachko, R. Miake-Lye, A. Petzold, C. Roof, M. Schaefer, U. Schumann, I. Waitz and R. Wayson (2010): Guidance on the use of AEDT gridded aircraft emissions in atmospheric models. MIT Laboratory for Aviation and the Environment **Rep. LAE-2010-008-N**, 13 pp. (http://lae.mit.edu/uploads/LAE_report_series/2010/LAE-2010-008-N.pdf)

Brasseur, G., M. Gupta, B. Anderson, S. Balasubramanian, S. Barrett, D. Duda, G. Fleming, P. Forster, J. Fuglestvedt, A. Gettelman, R. Halthore, S. Jacob, M. Jacobson, A. Khodayari, K. Liou, M. Lund, R. Miake-Lye, P. Minnis, S. Olsen, J. Penner, R. Prinn, U. Schumann, H. Selkirk, A. Sokolov, N. Unger, P. Wolfe, H. Wong, D. Wuebbles, B. Yi, P. Yang and C. Zhou (2016): Impact of Aviation on Climate: FAA's Aviation Climate Change Research Initiative (ACCRI) Phase II. *Bull Amer Meteor Soc* **97**, 561–583 (doi:10.1175/BAMS-D-13-00089.1)

Bonan, G.B., K.W. Oleson, M. Vertenstein, S. Lewis, X. Zeng, Y. Dai, R.E. Dickinson and Z.-L. Yang (2002): The land surface climatology of the Community Land Model coupled to the NCAR Community Climate Model. *J Climate* **15**, 3123–3149

Bony, S., R. Colman, V.M. Kattsov, R.P. Allan, C.S. Bretherton, J.-L. Dufresne, A. Hall, S. Hallegatte, M.M. Holland, W. Ingram, D.A. Randall, B.J. Soden, G. Tselioudis and M.J. Webb (2006): How well do we understand and evaluate climate change feedback processes? *J Climate* **19**, 3445–3482

Brovkin, V., M. Claussen, E. Driesschaert, T. Fichefet, D. Kicklighter, M.F. Loutre, H.D. Matthews, N. Ramankutty, M. Schaeffer and A. Sokolov (2006): Biogeophysical effects of historical land cover changes simulated by six Earth system models of intermediate complexity. *Climate Dyn* **26**, 587–600

Butterbach-Bahl, K., E.M. Baggs, M. Dannenmann, R. Kiese and S. Zechmeister-Boltenstern (2013): Nitrous oxide emissions from soils: how well do we understand the processes and their controls? *Phil Trans R Soc B* **368**: 20130122 (doi:10.1098/rstb.2013.0122)

Calbó, J., W. Pan, M. Webster, R.G. Prinn and G.J. McRae (1998): Parameterization of urban sub-grid scale processes in global atmospheric chemistry models. *J Geophys Res* **103**, 3437–3451

Cess R.D., G.L. Potter, J.P. Blanchet, G.J. Boer, A.D. Del Genio, M. Déqué, V. Dymnikov, V. Galin, W.L. Gates, S.J. Ghan, J.T. Kiehl, A.A. Lacis, H. Le Treut, Z.-X. Li, X.-Z. Liang, B.J. McAvaney, V.P. Meleshko, J.F.B. Mitchell, J.-J. Morcrette, D.A. Randall, L. Rikus, E. Roeckner, J.F. Royer, U. Schlese, D.A. Sheinin, A. Slingo, A.P. Sokolov, K.E. Taylor, W.M. Washington, R.T. Wetherald, I. Yagai, M.-H. Zhang (1990): Intercomparison and interpretation of climate feedback processes in 19 atmospheric general circulation models. *J Geophys Res* **95**, 16,601–16,615

Chen, M., Q. Zhuang, D.R. Cook, R. Coulter, M. Pekour, R.L. Scott, J.W. Munger and K. Bible (2011) Quantification of terrestrial ecosystem carbon dynamics in the conterminous United States combining a process-based biogeochemical model and MODIS and AmeriFlux data. *Biogeosciences* **8**, 2665–2688 (doi:10.5194/bg-8-2665-2011)

Cionni, I., V. Eyring, J.F. Lamarque, W.J. Randel, D.S. Stevenson, F. Wu, G.E. Bodeker, T.G. Shepherd, D.T. Shindell and D.W. Waugh (2011): Ozone database in support of CMIP5 simulations: Results and corresponding radiative forcing. *Atmos Chem Phys* **11**, 11,267–11,292

Claussen, M., L.A. Mysak, A.J. Weaver, M. Crucifix, T. Fichefet, M.-F. Loutre, S.L. Weber, J. Alcamo, V.A. Alexeev, A. Berger, R. Calov, A. Ganopolski, H. Goosse, G. Lohman, F. Lunkeit, I.I. Mokhov, V. Petoukhov, P. Stone and Z. Wang (2002): Earth system models of intermediate complexity: Closing the gap in the spectrum of climate system models. *Climate Dyn* **15**: 579–586

Collins, M., R. Knutti, J. Arblaster, J.-L. Dufresne, T. Fichefet, P. Friedlingstein, X. Gao, W.J. Gutowski, T. Johns, G. Krinner, M. Shongwe, C. Tebaldi, A.J. Weaver and M. Wehner (2013): Long-term Climate Change: Projections, Commitments and Irreversibility. In: *Climate Change 2013: The Physical Science Basis. Contribution of Working Group I to the Fifth Assessment Report of the Intergovernmental Panel on Climate Change* [Stocker, T.F., D. Qin, G.-K. Plattner, M. Tignor, S.K. Allen, J. Boschung, A. Nauels, Y. Xia, V. Bex and P.M. Midgley (eds.)]. Cambridge University Press, Cambridge, United Kingdom and New York, NY, USA

Colman, R. (2003): A comparison of climate feedbacks in general circulation models. *Climate Dyn* **20**, 865–873

Curtis, P.S. and X. Wang (1998): A meta-analysis of elevated CO_2 effects on woody plant mass, form, and physiology. *Oecologia* **113**, 299–313

Dutkiewicz. S., A. Sokolov, J. Scott and P. Stone (2005): *A Three-Dimensional Ocean-Seaice-Carbon Cycle Model and its Coupling to a Two-Dimensional Atmospheric Model: Uses in Climate Change Studies.* MIT Joint Program **Report 122** (https://globalchange.mit.edu/sites/default/files/MITJPSPGC_Rpt122.pdf)

Eby, M., A.J. Weaver, K. Alexander, K. Zickfeld, A. Abe-Ouchi, A. A. Cimatoribus, E. Crespin, S.S. Drijfhout, N. R. Edwards, A.V. Eliseev, G. Feulner, T. Fichefet, C.E. Forest, H. Goosse, P.B. Holden, F. Joos, M. Kawamiya , D. Kicklighter, H. Kienert, K. Matsumoto, I.I. Mokhov, E. Monier, S.M. Olsen, J.O.P. Pedersen, M. Perrette, G. Philippon-Berthier, A. Ridgwell, A. Schlosser, T. Schneider von Deimling, G. Shaffer, R. Smith, R. Spahni, A.P. Sokolov, M. Steinacher, K. Tachiiri, K. Tokos, M. Yoshimori, N. Zeng, and F. Zhao (2013): Historical and idealized climate model experiments: an intercomparison of Earth system models of intermediate complexity. *Clim Past* **9**, 1111–1140

Fant, C., C.A. Schlosser, X. Gao, K. Strzepek and J. Reilly (2016): Projections of water stress based on an ensemble of socioeconomic growth and climate change scenarios: a case study in Asia. *PLOS ONE* **11**(3): e0150633

Felzer, B., D. Kicklighter, J. Melillo, C. Wang, Q. Zhuang and R. Prinn (2004): Effects of ozone on net primary production and carbon sequestration in the conterminous United States using a biogeochemistry model. *Tellus B* **56**, 230–248 (doi:10.1111/j.1600-0889.2004.00097.x.)

Felzer, B., J. Reilly, J. Melillo, D. Kicklighter, M. Sarofim, C. Wang, R. Prinn and Q. Zhuang (2005): Future effects of ozone on carbon sequestration and climate change policy using a global biogeochemical model. *Climatic Change* **73**, 345–373 (doi:10.1007/s10584-005-6776-4)

Flato, G., J. Marotzke, B. Abiodun, P. Braconnot, S.C. Chou, W. Collins, P. Cox, F. Driouech, S. Emori, V. Eyring, C. Forest, P. Gleckler, E. Guilyardi, C. Jakob, V. Kattsov, C. Reason and M. Rummukainen (2013): Evaluation of Climate Models. In: *Climate Change 2013: The Physical Science Basis. Contribution of Working Group I to the Fifth Assessment Report of the Intergovernmental Panel on Climate Change* [Stocker, T.F., D. Qin, G.-K. Plattner, M. Tignor, S.K. Allen, J. Boschung, A. Nauels, Y. Xia, V. Bex and P.M. Midgley (eds.)]. Cambridge University Press, Cambridge, United Kingdom and New York, NY, USA

Follows, M.J., T. Ito and S. Dutkiewicz (2006): A Compact and Accurate Carbonate Chemistry Solver for Ocean Biogeochemistry Models. *Ocean Model* **12**, 290–301

Forest, C.E., P.H. Stone, A.P. Sokolov, M.R. Allen and M. Webster (2002): Quantifying uncertainties in climate system properties with the use of recent climate observations. *Science* **295**: 113–117

Forest, C.E., P.H. Stone and A.P. Sokolov (2008): Constraining Climate Model Parameters from Observed 20th Century Changes. *Tellus A* **60**, 911–920

Forster, P.M., T. Andrews, P. Good, J.M. Gregory, L.S. Jackson and M. Zelinka (2013): Evaluating adjusted forcing and model spread for historical and future scenarios in the CMIP5 generation of climate models. *J Geophys Res Atmos* **118**, 1139– 1150.

Friedlingstein, P., P. Cox, R. Betts, L. Bopp, W. von Bloh, V. Brovkin, P. Cadule, S. Doney, M. Eby, I. Fung, G. Bala, J. John, C. Jones, F. Joos, T. Kato, M. Kawamiya, W. Knorr, K. Lindsay, H.D. Matthews, T. Raddatz, P. Rayner, C. Reick, E. Roeckner, K.-G. Schnitzler, R. Schnur, K. Strassmann, A.J. Weaver, C. Yoshikawa and N. Zeng (2006): Climate–Carbon Cycle Feedback Analysis: Results from the CMIP4 Model Intercomparison. *J Climate* **19**, 3337–3353

Friedlingstein, P., M. Meinshausen, V.K. Arora, C.D. Jones, A. Anav, S.K. Liddicoat, R. Knutti (2014): Uncertainties in CMIP5 Climate Projections due to Carbon Cycle Feedbacks. *J Climate* **27**, 511–526 (doi:10.1175/JCLI-D-12-00579.1)

Galford, G.L., J.M. Melillo, D.W. Kicklighter, T.W. Cronin, C.E.P. Cerri, J.F. Mustard and C.C. Cerri (2010): Greenhouse gas emissions from alternative futures of deforestation and agricultural management in the southern Amazon. *PNAS* **107**, 19,649–19,654 (doi:10.1073/pnas.1000780107)

Galford, G.L., J.M. Melillo, D.W. Kicklighter, J.F. Mustard, T.W. Cronin, C.E.P. Cerri and C.C. Cerri (2011): Historical carbon emissions and uptake from the agricultural frontier of the Brazilian Amazon. *Ecological Applications* **21**, 750–763 (doi:10.1890/09-1957.1.)

Gao X., C.A. Schlosser, A.P. Sokolov, K.W. Anthony, Q. Zhuang, D. Kicklighter (2013): Permafrost degradation and methane: low risk of biogeochemical climate-warming feedback. *Environ Res Lett* **8**, 035014

Gelaro, R., W. McCarty, M.J. Suárez, R. Todling, A. Molod, L. Takacs, C.A. Randles, A. Darmenova, M.G. Bosilovich, R. Reichle, K. Wargan, L. Coy, R. Cullather, C. Draper, S. Akella, V. Buchard, A. Conaty, A.M. da Silva, W. Gu, G.-K. Kim, R. Koster, R. Lucchesi, D. Merkova, J.E. Nielsen, G. Partyka, S. Pawson, W. Putman, M. Rienecker, S.D. Schubert, M. Sienkiewicz and B. Zhao (2017): The Modern-Era Retrospective Analysis for Research and Applications, Version 2 (MERRA-2). *J Climate*, online first (doi:10.1175/JCLI-D-16-0758.1)

Gillet, N.P., V.K. Arora, D. Matthews and M.R. Allen (2013): Constraining the ratio of global warming to cumulative CO_2 emissions using CMIP5 simulations. *J Climate* **26**, 6844–6858

Green, W.H. and G.A. Ampt (1911): Studies on soil physics, 1: The flow of air and water through soils. *J Agric Sci* **4**, 1–24

Gregory, J.M., R.J. Stouffer, S.C.B. Raper, P.A. Stott and N.A. Rayner (2002): An observationally based estimate of the climate sensitivity. *J Climate* **15**: 3117–3121

Gregory J.M., K.W. Dixon, R.J. Stouffer, A.J. Weaver, E. Driesschaert, E. Eby, T. Fichefet, H. Hasumi, A. Hu, J. Jungclause, I.V. Kamenkovich, A. Levermann, M. Montoya, S. Murakami, S. Nawrath, A. Oka, A. Sokolov, R.B. Trorpe (2005): A model intercomparison of changes in the Atlantic thermohaline circulation in response to increasing atmospheric CO_2 concentration. *Geophys Res Lett* **32**, L12703

Gunderson, C.A. and S.D. Wullschleger (1994): Photosynthetic acclimation in trees to rising atmospheric CO_2: a broader perspective. *Photosynthesis Res* **39**, 369–388

Hallgren, W., C.A. Schlosser, E. Monier, D. Kicklighter, A. Sokolov and J. Melillo (2013): Climate impacts of a large-scale biofuels expansion. *Geophys Res Lett* **40**, 1624–1630 (doi:10.1002/grl.50352)

Hansen, J., M. Sato, L. Nazarenko, R. Ruedy, A. Lacis, D. Koch, I. Tegen, T. Hall, D. Shindell, B. Santer, P. Stone, T. Novakov, L. Thomason, R. Wang, Y. Wang, D. Jacob, S. Hollandsworth, L. Bishop, J. Logan, A. Thompson, R. Stolarski, J. Lean, R. Willson, S. Levitus, J. Antonov, N. Rayner, D. Parker and J. Christy (2002): Climate forcings in Goddard Institute for Space Studies SI2000 simulations. *J Geophys Res* **107**, 4347

Hansen, J., I. Fung, A. Lacis, D. Rind, S. Lebedeff, R. Ruedy and G. Russell (1988): Global climate change as forecast by Goddard Institute for Space Studies three-dimensional model. *J Geophys Res* **93**, 9341–9364

Hansen, J., A. Lacis, D. Rind, G. Russell, P. Stone, I. Fung, R. Ruedy and J. Lerner (1984): Climate Sensitivity: Analysis of Feedback Mechanisms. In*: Climate Processes and Climate Sensitivity, Geophysical Monograph* [Hansen, J.E. and T. Takahashi, (eds.)], **29**. American Geophysical Union, Washington, D.C.

Hansen, J., G. Russell, D. Rind, P. Stone, A. Lacis, S. Lebedeff, R. Ruedy and L. Travis (1983): Efficient three-dimensional global models for climate studies: Models I and II. *Monthly Weather Review* **111**, 609–662

Hansen J, A. Lacis, R. Ruedy, M. Sato and H. Wilson (1993): How sensitive is world's climate? *National Geographic Research and Exploration* **9**, 142–158

Hansen, J., M. Sato, R. Ruedy, P. Kharecha, A. Lacis, R. Miller, L. Nazarenko, K. Lo, G. A. Schmidt, G. Russell, I. Aleinov, S. Bauer, E. Baum, B. Cairns, V. Canuto, M. Chandler, Y. Cheng, A. Cohen, A. Del Genio, G. Faluvegi, E. Fleming, A. Friend, T. Hall, C. Jackman, J. Jonas, M. Kelley, N. Y. Kiang, D. Koch, G. Labow, J. Lerner, S. Menon, T. Novakov, V. Oinas, Ja. Perlwitz, Ju. Perlwitz, D. Rind, A. Romanou, R. Schmunk, D. Shindell, P. Stone, S. Sun, D. Streets, N. Tausnev, D. Thresher, N. Unger, M. Yao and S. Zhang (2007): Climate simulations for 1880–2003 with GISS modelE. *Climate Dyn* **29** (doi:10.1007/s00382-007-0255-8)

Holian, G.L., A.P. Sokolov and R.G. Prinn (2001): *Uncertainty in Atmospheric CO_2 Predictions from a Global Ocean Carbon Cycle Model.* MIT Joint Program **Report 80**, 25 pp. (https://globalchange.mit.edu/sites/default/files/MITJPSPGC_Rpt80.pdf)

IPCC (2013): Climate change 2013: The physical science basis. Contribution of Working Group I to the *Fifth Assessment Report of the Intergovernmental Panel on Climate Change* (T.F. Stocker, D. Qin, G.K. Plattner, M. Tignor, S.K. Allen, J. Boschung, A. Nauels, Y. Xia, V. Bex and P.M. Midgley, eds). Cambridge: Cambridge University Press

Kamenkovich, I.V., A. Sokolov and P.H. Stone (2002): An efficient climate model with a 3D ocean and statistical-dynamical atmosphere. *Climate Dyn* **19**(7): 585–598

Kicklighter, D.W., A.C. Gurgel, J.M. Melillo, J.M. Reilly and S. Paltsev (2012): *Potential Direct and Indirect Effects of Global Cellulosic Biofuel Production on Greenhouse Gas Fluxes from Future Land-use Change.* MIT Joint Program on Science and Policy of Global Change **Report 210**. Massachusetts Institute of Technology, Cambridge, Massachusetts. (http://globalchange.mit.edu/files/document/MITJPSPGC_Rpt210.pdf).

Kicklighter, D.W., Y. Cai, Q. Zhuang, E.I. Parfenova, S. Paltsev, A.P. Sokolov, J.M. Melillo, J.M. Reilly, N.M. Tchebakova and X. Lu (2014): Potential influence of climate-induced vegetation shifts on future land use and associated land carbon fluxes in Northern Eurasia. *Environ Res Lett* **9**, 035004 (doi:10.1088/1748-9326/9/3/035004)

Klimont, Z., S.J. Smith and J. Cofala (2013): The last decade of global anthropogenic sulfur dioxide: 2000–2011 emissions. *Environ Res Lett* **8** (doi:10.1088/1748–9326/8/1/014 003)

Knutti, R., T.F. Stoker, F. Joos and G.-K. Plattner (2003): Probabilistic climate change projections using neural network. *Climate Dyn* **21**, 257–272

Kopp, G. and J.L. Lean (2011): A new, lower value of total solar irradiance: Evidence and climate significance. G*eophys Res Lett* **38** (L01706) (doi:10.1029/2010GL045 777)

Lawrence, D.M., K.W. Oleson, M.G. Flanner, P.E. Thornton, S.C. Swenson, P.J. Lawrence, X. Zeng, Z.-L. Yang, S. Levis, K. Sakaguchi, G.B. Bonan and A.G. Slater (2011): Parameterization improvements and functional and structural advances in version 4 of the Community Land Model. *J Adv Model Earth Syst* **3** (doi:10.1029/2011MS000045)

Le Quéré, C. *et al.* (2016): Global Carbon Budget 2016. *Earth Syst Sci Data* **8**, 605–649 (doi:10.5194/essd-8-605-2016)

Libardoni A. (2017): *Improving constraints on climate system properties with additional data and new methods.* A Dissertation in Meteorology. The Pennsylvania State University, The Graduate School, College of Earth and Mineral Science

Libardoni, A.G. and C.E. Forest (2011): Sensitivity of distributions of climate system properties to the surface temperature dataset. *Geophys. Res. Let.,* **38** (L22705) (doi:10.1029/2011GL049 431)

Libardoni, A.G. and C.E. Forest (2013): Correction to "sensitivity of distributions of climate system properties to the surface temperature data set". Geophys. Res. Let., **40** (doi:10.1002/grl.50 480)

Liu, Y. (1996): *Modeling the Emissions of Nitrous Oxide (N2O) and Methane (CH4) from the Terrestrial Biosphere to the Atmosphere.* Ph.D. Thesis, MIT. MIT Joint Program **Report 10**, Cambridge, MA, 219 p.

Lu, X., D.W. Kicklighter, J.M. Melillo, J.M. Reilly and L. Xu (2015): Land carbon sequestration within the conterminous United States: regional- and state-level analyses. *J Geophys Res-Biogeosciences* **120**(2): 379–398 (doi:10.1002/2014JG002818)

Matthews H.D., N.P. Gillett, P.A Stott and K. Zickfeld (2009): The proportionality of global warming to cumulative carbon emissions. *Nature* **2**, 459:829–832 (doi:10.1038/nature08047)

Mayer, M., C. Wang, M. Webster and R.G. Prinn (2000): Linking local air pollution to global chemistry and climate. *J Geophys Res* **105**, 22869–22896

McGuire, A.D., J.M. Melillo, L.A. Joyce, D.W. Kicklighter, A.L. Grace, B. Moore III and C.J. Vorosmarty (1992): Interactions between carbon and nitrogen dynamics in estimating net primary productivity for potential vegetation in North America. *Global Biogeochem Cycles* **6**, 101–124

McGuire, A.D., J.M. Melillo and L.A. Joyce (1995): The role of nitrogen in the response of forest net primary production to elevated atmospheric carbon dioxide. *Annual Review of Ecology and Systematics* **26**, 473–503

McGuire A.D., J.M. Melillo, D.W. Kicklighter, Y. Pan, X. Xiao, J. Helfrich, B. Moore III, C.J. Vorosmarty and A.L. Schloss (1997): Equilibrium responses of global net primary production and carbon storage to doubled atmospheric carbon dioxide: sensitivity to changes in vegetation nitrogen concentration. *Global Biogeochem Cycles* **11**, 173–189

McGuire, A.D., S. Sitch, J.S. Clein, R. Dargaville, G. Esser, J. Foley, M. Heimann, F. Joos, J. Kaplan, D.W. Kicklighter, R.A. Meier, J.M. Melillo, B. Moore III, I.C. Prentice, N. Ramankutty, T. Reichenau, A. Schloss, H. Tian, L.J. Williams and U. Wittenberg (2001): Carbon balance of the terrestrial biosphere in the twentieth century: analyses of CO_2, climate and land-use effects with four process-based ecosystem models. *Global Biogeochem Cycles* **15**(1): 183–206 (doi:10.1029/2000GB001298)

Meinshausen, M., S. Raper and T. Wigley (2011): Emulating coupled atmosphere-ocean and carbon cycle models with a simpler model, MAGICC6–Part 1: Model description and calibration. *Atmos Chem Phys* **11**, 1417–1456.

Melillo, J.M., A.D. McGuire, D.W. Kicklighter, B. Moore III, C.J. Vorosmarty and A.L. Schloss (1993): Global climate change and terrestrial net primary production. *Nature* **363**, 234–240

Melillo, J.M., J.M. Reilly, D.W. Kicklighter, A.C. Gurgel, T.W. Cronin, S. Paltsev, B.S. Felzer, X. Wang, A.P. Sokolov and C.A. Schlosser (2009): Indirect emissions from biofuels: how important? *Science* **326**, 1397–1399 (doi:10.1126/science.1180251)

Melillo, J.M., X. Lu, D.W. Kicklighter, J.M. Reilly, Y. Cai and A.P. Sokolov (2016) Protected areas' role in climate-change mitigation. *Ambio* **45**(2), 133–145 (doi:10.1007/s13280-015-0693-1)

Melton, J.R., R. Wania, E.L. Hodson, B. Poulter, B. Ringeval, R. Spahni, T. Bohn, C.A. Avis, D.J. Beerling, G. Chen, A.V. Eliseev, S.N. Denisov, P.O. Hopcroft, D.P. Lettenmaier, W.J. Riley, J.S. Singarayer, Z.M. Subin, H. Tian, S. Zürcher, V. Brovkin, P.M. van Bodegom, T. Kleinen, Z.C. Yu and J.O. Kaplan (2013): Present state of global wetland extent and wetland methane modelling: conclusions from a model inter-comparison project (WETCHIMP). *Biogeosciences*, **10**, 753–788 (doi:10.5194/bg-10-753-2013)

Miller, R.L., G.A. Schmidt, L.S. Nazarenko, N. Tausnev, S.E. Bauer, A.D. DelGenio, M. Kelley, K.K. Lo, R. Rudy, D.T. Shindell, I. Aleinov, M. Bauer, Rainer Bleck, V. Canuto, Y. Chen, Y. Cheng, T.L. Clune, G. Faluvegi, J.E. Hansen, R.J. Healy, N.Y. Kiang, D. Koch, A.A. Lacis, A.N. LeGrande, J. Lerner, S. Menon, V. Oinas, C. Pérez García-Pando, J.P. Perlwitz, M.J. Puma, D. Rind, A. Romanou, G.L. Russell, M. Sato, S. Sun, K. Tsigaridis, N. Unger, A Voulgarakis, M.-S. Yao and J. Zhang (2014): CMIP5 historical simulations (1850–2012) with GISS model E2. *J Adv Model Earth Syst.* **6**, 441–477

Monier, E., A.P. Sokolov, C.A. Schlosser, J.R. Scott and X. Gao (2013): Probabilistic projections of 21st century climate change over Northern Eurasia. *Environ Res Lett* **8**, 045008

Monier, E., X. Gao, J.R. Scott, A.P. Sokolov and C.A. Schlosser (2015): A framework for modeling uncertainty in regional climate change. C*limatic Change*, **131**(1), 51–66

Morice, C.P., J.J. Kennedy, N.A. Rayner and P.D. Jones (2012): Quantifying uncertainties in global and regional temperature change using an ensemble of observational estimates: The HadCRUT4 dataset. *J Geophys Res* **117**, D08101 (doi:10.1029/2011JD017187)

Norby, R.J., S.D. Wullschleger, C.A. Gunderson, D.W. Johnson and R. Ceulemans (1999): Tree responses to rising CO_2: implications for the future forest. *Plant, Cell and Environment* **22**, 683–714

Norby, R.J., E.H. DeLucia, B. Gielen, C. Calfapietra, C.P. Giardina, J.S. King, J. Ledford, H.R. McCarthy, D.J.P. Moore, R. Ceulemans, P. De Angelis, A.C. Finzi, D.F. Karnosky, M.E. Kubiske, M. Lukac, K.S. Pregitzer, G.E. Scarascia-Mugnozza, W.H. Schlesinger and R. Oren (2005): Forest response to elevated CO_2 is conserved across a broad range of productivity. *PNAS* **102**, 18052–18056

Oleson, K.W., D.M. Lawrence, G.B. Bonan, M.G. Flanner, E. Kluzek, P.J. Lawrence, S. Levis, S.C. Swenson, P.E. Thornton, A. Dai, M. Decker, R. Dickinson, J. Feddema, C.L. Heald, F. Hoffman, J.-F. Lamarque, N. Mahowald, G.-Y. Niu, T. Qian, J. Randerson, S. Running, K. Sakaguchi, A. Slater, R. Stockli, A. Wang, Z.-L. Yang, Xi. Zeng and Xu. Zeng (2010): *Technical Description of version 4.0 of the Community Land Model (CLM)*. NCAR Technical Note NCAR/TN-478+STR, National Center for Atmospheric Research, Boulder, CO, 257 pp.

Olsen S., G. Brasseur, D. Wuebbles, S. Barrett, H. Dang, S. Eastham, M. Jacobson, A. Khodayari, H. Selkirk, A. Sokolov and N. Unger (2013): Comparison of model estimates of the effects of aviation emissions on atmospheric ozone and methane. *Geophys Res Lett* **40**, 6004–6009

Paltsev, S., J.M. Reilly, H.D. Jacoby, R.S. Eckaus, J. McFarland, M. Sarofim, M. Asadoorian and M. Babiker (2005): *The MIT Emissions Prediction and Policy Analysis (EPPA) Model: Version 4*. MIT Joint Program **Report 125**, 72 pp. (https://globalchange.mit.edu/sites/default/files/MITJPSPGC_Rpt125.pdf)

Pan, Y., J.M. Melillo, A.D. McGuire, D.W. Kicklighter, L.F. Pitelka, K. Hibbard, L.L. Pierce, S.W. Running, D.S. Ojima, W.J. Parton, D.S. Schimel and other VEMAP Members (1998): Modeled responses of terrestrial ecosystems to elevated atmospheric CO_2: A comparison of simulations by the biogeochemistry models of the Vegetation/Ecosystem Modeling and Analysis Project (VEMAP). *Oecologia* **114**, 389–404

Peixoto, J.P. and A.H. Oort (1992): Physics of Climate. AIP, New York, 520 pp.

Petoukhov, V. , A. Berger, T. Fichefet, H. Goosse, M. Crucifix, M. Eby, A.J. Weaver, A.V. Eliseev, I.I. Mokhov, I. Kamenkovich, M. Montoya, L.A. Mysak, Z. Wang, A. Sokolov and P. Stone (2005): EMIC Intercomparison Project (EMIPCO_2): Comparative analysis of EMIC simulations of climate, and of equilibrium and transient responses to atmospheric CO_2 doubling. *Clim Dyn* (doi:10.1007/s00382-00005-00042-00383)

Plattner G. and Coauthors (2008): Long-Term Climate Commitments Projected with Climate-Carbon Cycle Models. *J Climate* **21** 2721–2751

Prinn, R., H. Jacoby, A. Sokolov, C. Wang, X. Xiao, Z. Yang, R. Eckaus, P. Stone, D. Ellerman, J. Melillo, J. Fitzmaurice, D. Kicklighter, G. Holian and Y. Liu (1999): Integrated global system model for climate policy assessment: Feedbacks and sensitivity studies. *Climatic Change* **41**: 469–546

Prinn, R., J. Reilly, M. Sarofim, C. Wang and B. Felzer (2007): Effects of air pollution control on climate: results from an integrated assessment model. in: *Human-induced Climate Change: An Interdisciplinary Assessment* [M.E. Schlesinger, H.S. Kheshgi, J. Smith, F.C. de la Chesnaye, J.M. Reilly, T. Wilson and C. Kolstad (eds.)]. Cambridge University Press, Cambridge, UK

Pu, B. and R.E. Dickinson (2012): Examining vegetation feedbacks on global warming in the Community Earth System Model. *J Geophys Res-Atmospheres* **117**

Raich, J.W., E.B. Rastetter, J.M. Melillo, D.W. Kicklighter, P.A. Steudler, B.J. Peterson, A.L. Grace, B. Moore III and C.J. Vorosmarty (1991): Potential net primary productivity in South America: application of a global model. *Ecological Applications* **1**, 399–429

Raper, S.C.B., J.M. Gregory and T.J. Osborn (2001): Use of an upwelling-diffusion energy balance climate model to simulate and diagnose A/OGCM results*, Climate Dyn*, **17**, 601–613

Raper, C.S.B., J.M. Gregory and R.J. Stouffer (2002): The role of climate sensitivity and ocean heat uptake on AOGCM transient temperature and thermal expansion response. *J Climate* **15**, 124–130

Reilly, J., S. Paltsev, B. Felzer, X. Wang, D. Kicklighter, J. Melillo, R. Prinn, M. Sarofim, A. Sokolov and C. Wang (2007): Global economic effects of changes in crops, pasture and forests due to changing climate, carbon dioxide and ozone. *Energy Policy* **35**, 5370–5383 (doi:10.1016/j.enpol.2006.01.040)

Reilly, J., J. Melillo, Y. Cai, D. Kicklighter, A. Gurgel, S. Paltsev, T. Cronin, A. Sokolov and A. Schlosser (2012): Using land to mitigate climate change: hitting the target, recognizing the tradeoffs. *Environ Sci Technol* **46**(11), 5672–5679 (doi:10.1021/es2034729)

Rogelj, J., M. Meinshausen and R. Knutti (2012): Global warming under old and new scenarios using IPCC climate sensitivity range estimates, *Nat. Clim. Change*, **2**, 248–53

Russell, G.L., J.R. Miller and L-C Tsang (1985): Seasonal ocean heat transport computed from an atmospheric model. *Dyn. Atmos. Oceans*, **9**, 253–271

Saikawa, E., C.A. Schlosser and R.G. Prinn (2013): Global modeling of soil N2O emissions from natural processes*, Global Biogeochem Cycles*, online first (doi:10.1002/gbc.20087)

Sato, M., J.E. Hansen, M.P. McCormick and J.B. Pollack (1993): Stratospheric aerosol optical depths. *J Geophys Res*, **98** (D12), 22,987–22,944

Schlosser, C.A., D. Kicklighter and A. Sokolov (2007): *A global land system framework for integrated climate-change assessments*. MIT Joint Program **Report 147**, 82 pp. (https://globalchange.mit.edu/sites/default/files/MITJPSPGC_Rpt147.pdf)

Schlosser, C.A., X. Gao, K. Strzepek, A. Sokolov, C.E. Forest, S. Awadalla and W. Farmer (2013): Quantifying the likelihood of regional climate change: a hybridized approach. *J Climate* **26**(10), 3394–3414

Smith, T.M., P.A. Arkin, L. Ren and S.S. Shen (2012): Improved reconstruction of global precipitation since 1900. *J Atmos Ocean Tech* **29**, 1505–1517

Sokolov, A.P. (2006): Does Model Sensitivity to Changes in CO_2 Provide a Measure of Sensitivity to Other Forcings? *J Climate* **19**(13): 3294–3306

Sokolov, A.P., C.E. Forest and P.H. Stone (2003): Comparing oceanic heat uptake in AOGCM transient climate change experiments. *J Climate* **16**: 1573–1582

Sokolov, A.P and E. Monier (2012): Changing the Climate Sensitivity of an Atmospheric General Circulation Model Trough Cloud Radiative Adjustment. *J Climate* **25** (19): 6567–6584

Sokolov, A.P. and P.H. Stone (1995): *Description and validation of the MIT version of the GISS 2-D model*. MIT Joint Program **Report 2**, 23 pp. (https://globalchange.mit.edu/publication/13844)

Sokolov, A. and P.H. Stone (1998): A flexible climate model for use in integrated assessments. *Climate Dyn*, **14**: 291–303

Sokolov, A.P., C.A. Schlosser, S. Dutkiewicz, S. Paltsev, D.W. Kicklighter, H.D. Jacoby, R.G. Prinn, C.E. Forest, J. Reilly, C. Wang, B. Felzer, M.C. Sarofim, J. Scott, P.H. Stone, J.M. Melillo and J. Cohen (2005): *The MIT Integrated Global System Model (IGSM) Version 2: Model Description and Baseline Evaluation*. MIT Joint Program **Report 124**, 40 pp. (https://globalchange.mit.edu/sites/default/files/MITJPSPGC_Rpt124.pdf)

Sokolov, A.P., S. Dutkiewicz, P.H. Stone and J.R. Scott (2007): *Evaluating the use of ocean models of different complexity in climate change studies*. MIT Joint Program **Report 128**, 23 pp. (https://globalchange.mit.edu/sites/default/files/MITJPSPGC_Rpt128.pdf)

Sokolov, A., P.H. Stone, C.E. Forest, R.G. Prinn, M.C.Sarofim, M. Webster, S. Paltsev, C.A. Schlosser, D. Kicklighter, S.Dutkiewicz, J. Reilly, C. Wang, B. Felzer,and H.D. Jacoby (2009): Probabilistic forecast for 21st century climate based on uncertainties in emissions (without policy) and climate parameters. *J Climate* **22**(19): 5175–5204

Stocker, T.F., W.S. Broecker and D.G. Wright (1994): Carbon Uptake Experiments with a Zonally-Averaged Global Ocean Circulation Model. *Tellus* **46B**, 103–122

Stone, P.H. and M.-S. Yao (1990): Development of a two-dimensional zonally averaged statistical-dynamical model. III: The parameterization of the eddy fluxes of heat and moisture. *J Climate* **3**: 726–740

Stone, P.H. and M.-S. Yao (1987): Development of a two-dimensional zonally averaged statistical-dynamical model. II: The role of eddy momentum fluxes in the general circulation and their parameterization. *J. Atmospheric Science* **44**: 3769–3536

Stouffer, R.J., J. Yin, J.M. Gregory, K.W. Dixon, M.J. Spelman, W. Hurlin, A.J. Weaver, E. Eby, G.M. Flato, H. Hasumi, A. Hu, J. Jungclause, I.V. Kamenkovich, A. Levermann, M. Montoya, S. Murakami, S. Nawrath, A. Oka, W.R. Peltier, D.Y. Bobitaille, A. Sokolov, G. Vettoretti, N. Weber (2006): Investigating the Causes of the Response of the Thermohaline Circulation to Past and Future Climate Changes. *J Climate* **19**, 1365–1387

Swenson, S.C., D.M. Lawrence and H. Lee (2012): Improved simulation of the terrestrial hydrological cycle in permafrost regions by the Community Land Model. *J Adv Model Earth Syst* **4**: M08002

Tatang, M.A., W. Pan, R.G. Prinn and G.J. McRae (1997): An efficient method for parametric uncertainty analysis of numerical geophysical models. *J Geophys Res* **102**: 21925–21932

Taylor K.E., R.J. Stouffer and G.A. Meehl (2012): An overview of CMIP5 and the experiment design. *Bull Amer Meteor Soc*, **93**, 485 – 98

Tian, H., J.M. Melillo, D.W. Kicklighter, A.D. McGuire and J. Helfrich (1999): The sensitivity of terrestrial carbon storage to historical climate variability and atmospheric CO_2 in the United States. *Tellus B* **51**(2), 414–452 (doi:10.1034/j.1600-0889.1999.00021.x)

Tseng, Y.H., S.-H. Chien, J. Jin and N.L. Miller (2012): Modeling Air-Land-Sea Interactions Using the Integrated Regional Model System in Monterey Bay, California. *Monthly Weather Review* **140**(4): 1285–1306

Vano, J.A, T. Das and D.P. Lettenmaier (2012): Hydrologic Sensitivities of Colorado River Runoff to Changes in Precipitation and Temperature. *J Hydrometeorol* **13** (3): 932–949

Wang, C. (2004): A modeling study on the climate impacts of black carbon aerosols. *J Geophys Res* **109** (D03106) (doi:10.1029/2003JD004084)

Wang, C., R.G. Prinn and A. Sokolov (1998): A global interactive chemistry and climate model: Formulation and testing. *J Geophys Res* **103**, 3399–3418

Webb, M.J., C.A. Senior, D.M.H. Sexton, W.J. Ingram, K.D. Williams, M.A. Ringer, B.J. McAvaney, R.Colman, B.J. Soden, R. Gudgel, T. Knutson, S. Emori, T. Ogura, Y. Tsushima, N. Andronova, B. Li, I. Musat, S. Bony and K.E. Taylor (2006): On the contribution of local feedback mechanisms to the range of climate sensitivity in two GCM ensembles. *Climate Dyn* **27**(1), 17–38 (doi:10.1007/s00382-006-0111-2)

Webster, M.D., M. Babiker, M. Mayer, J.M. Reilly, J. Harnisch, R. Hyman, M.C. Sarofim and C. Wang (2002): Uncertainty in emissions projections for climate models. *Atmospheric Environment* **36**, 3659–3670

Webster, M., C. Forest, J. Reilly, M. Babiker, D. Kicklighter, M. Mayer, R. Prinn, M. Sarofim, A. Sokolov, P. Stone and C. Wang (2003): Uncertainty analysis of climate change and policy response. *Climatic Change* **62**, 295–320

Webster, M.D., S. Paltsev, J. Parsons, J. Reilly and H. Jacoby (2008): *Uncertainty in greenhouse emissions and costs of atmospheric stabilization*. MIT JPSPGC **Report 165**. (https://globalchange.mit.edu/sites/default/files/MITJPSPGC_Rpt165.pdf)

Webster, M., A. Sokolov, J. Reilly, C. Forest, S. Paltsev, A. Schlosser, C. Wang, D. Kicklighter, M. Sarofim, J. Melillo, R. Prinn, H. Jacoby (2012): Analysis of Climate Policy Targets under Uncertainty. *Climatic Change* **112**, 569–583

Williams, K.D., M.A. Ringer, C.A. Senior, M.J. Webb, B.J. McAvaney, N. Andronova, S. Bony, J.-L. Dufresne, S. Emori, R. Gudgel, T. Knutson, B. Li, K. Lo, I. Musat, J. Wegner, A. Slingo and J.F.B. Mitchell (2006): Evaluation of a component of the cloud response to climate change in an intercomparison of climate models. *Climate Dyn* **26** (2–3), 145–165 (doi:10.1007/s00382-005-0067-7)

Xiao, X., J.M. Melillo, D.W. Kicklighter, A.D. McGuire, R.G. Prinn, C. Wang, P.H. Stone and A. Sokolov (1998): Transient climate change and net ecosystem production of the terrestrial biosphere. *Global Biogeochem Cycles* **12**, 345–360

Xiao, X., D.W. Kicklighter, J.M. Melillo, A.D. McGuire, P.H. Stone and A.P. Sokolov (1997): Linking a global terrestrial biogeochemical model and a 2-dimensional climate model: Implications for the global carbon budget. *Tellus B* **49**, 18–37

Xin, Y.F., B.Y. Wu, L.G. Bian, G. Liu, L. Zhang and R. Li (2012): Response of the East Asian climate system to water and heat changes of global frozen soil using NCAR CAM model. *Chinese Science Bulletin* **57**(34): 4462–4471

Zampieri, M., E. Serpetzoglou, E.N. Anagnostoua, E.I. Nikolopoulos and A. Papadopoulos (2012): Improving the representation of river-groundwater interactions in land surface modeling at the regional scale: Observational evidence and parameterization applied in the Community Land Model. *Journal of Hydrology* **420**: 72–86

Zhang, S.L., J. Shi and Y. Dou (2012): A soil moisture assimilation scheme based on the microwave Land Emissivity Model and the Community Land Model. *International Journal of Remote Sensing* **33**(9): 2770–2797

Zhu, X., Q. Zhuang, M. Chen, A. Sirin, J. Melillo, D. Kicklighter, A. Sokolov and L. Song (2011): Rising methane emissions in response to climate change in Northern Eurasia during the 21st century. *Environ Res Lett* **6**(4): 1–9 (doi:10.1088/1748-9326/6/4/045211)

Zhu, Q. and Q. Zhuang (2013): Modeling the effects of organic nitrogen uptake by plants on the carbon cycling of boreal forest and tundra ecosystems. *Biogeosciences* **10**, 7943–7955 (doi:10.5194/bg-10-7943-2013)

Zhu, X., Q. Zhuang, Z. Qin, M. Glagolev and L. Song (2013): Estimating wetland methane emissions from the northern high latitudes from 1990 to 2009 using artificial neural networks. *Global Biogeochem Cycles* **27**, 592–604 (doi:10.1002/gbc.20052)

Zhuang, Q., J.M. Melillo, D.W. Kicklighter, R.G. Prinn, A.D. McGuire, P.A. Steudler, B.S. Felzer and S. Hu (2004): Methane fluxes between terrestrial ecosystems and the atmosphere at northern high latitudes during the past century: A retrospective analysis with a process-based biogeochemistry model. *Global Biogeochem Cycles* **18**, GB3010 (doi:10.1029/2004GB002239)

Zickfeld, K., M. Eby, A.J. Weaver, K. Alexander, E. Crespin, N.R. Edwards, Al.V. Eliseev, G. Feulner, T. Fichefet, C.E. Forest, P. Friedlingstein, H. Goosse, P.B. Holden, F. Joos, M. Kawamiya, D. Kicklighter, H. Kienert, K. Matsumoto, I.I. Mokhov, E. Monier, S.M. Olsen, J.O.P. Pedersen, M. Perrette, G. Philippon-Berthier, A. Ridgwell, A. Schlosser, T. Schneider Von Deimling, G. Shaffer, A. Sokolov, R. Spahni, M. Steinacher, K. Tachiiri, K.S. Tokos, M. Yoshimori, N. Zeng and F. Zhao (2013): Long-Term climate Change Commitment and Reversibility: An EMIC Intercomparison. *J Climate* **26**, 5782–5809.

Joint Program Report Series - Recent Articles

For limited quantities, Joint Program Reports are available free of charge. Contact the Joint Program Office to order.
Complete list: http://globalchange.mit.edu/publications

325. **Description and Evaluation of the MIT Earth System Model (MESM).** *Sokolov et al., Feb 2018*

324. **Finding Itself in the Post-Paris World: Russia in the New Global Energy Landscape.** *Makarov et al., Dec 2017*

323. **The Economic Projection and Policy Analysis Model for Taiwan: A Global Computable General Equilibrium Analysis.** *Chai et al., Nov 2017*

322. **Mid-Western U.S. Heavy Summer-Precipitation in Regional and Global Climate Models: The Impact on Model Skill and Consensus Through an Analogue Lens.** *Gao and Schlosser, Oct 2017*

321. **New data for representing irrigated agriculture in economy-wide models.** *Ledvina et al., Oct 2017*

320. **Probabilistic projections of the future climate for the world and the continental USA.** *Sokolov et al., Sep 2017*

319. **Estimating the potential of U.S. urban infrastructure albedo enhancement as climate mitigation in the face of climate variability.** *Xu et al., Sep 2017*

318. **A Win-Win Solution to Abate Aviation CO_2 emissions.** *Winchester, Aug 2017*

317. **Application of the Analogue Method to Modeling Heat Waves: A Case Study With Power Transformers.** *Gao et al., Aug 2017*

316. **The Revenue Implications of a Carbon Tax.** *Yuan et al., Jul 2017*

315. **The Future Water Risks Under Global Change in Southern and Eastern Asia: Implications of Mitigation.** *Gao et al., Jul 2017*

314. **Modeling the Income Dependence of Household Energy Consumption and its Implications for Climate Policy in China.** *Caron et al., Jul 2017*

313. **Global economic growth and agricultural land conversion under uncertain productivity improvements in agriculture.** *Lanz et al., Jun 2017*

312. **Can Tariffs be Used to Enforce Paris Climate Commitments?** *Winchester, Jun 2017*

311. **A Review of and Perspectives on Global Change Modeling for Northern Eurasia.** *Monier et al., May 2017*

310. **The Future of Coal in China.** *Zhang et al., Apr 2017*

309. **Climate Stabilization at 2°C and Net Zero Carbon Emissions.** *Sokolov et al., Mar 2017*

308. **Transparency in the Paris Agreement.** *Jacoby et al., Feb 2017*

307. **Economic Projection with Non-homothetic Preferences: The Performance and Application of a CDE Demand System.** *Chen, Dec 2016*

306. **A Drought Indicator based on Ecosystem Responses to Water Availability: The Normalized Ecosystem Drought Index.** *Chang et al., Nov 2016*

305. **Is Current Irrigation Sustainable in the United States? An Integrated Assessment of Climate Change Impact on Water Resources and Irrigated Crop Yields.** *Blanc et al., Nov 2016*

304. **The Impact of Oil Prices on Bioenergy, Emissions and Land Use.** *Winchester & Ledvina, Oct 2016*

303. **Scaling Compliance with Coverage? Firm-level Performance in China's Industrial Energy Conservation Program.** *Karplus et al., Oct 2016*

302. **21st Century Changes in U.S. Heavy Precipitation Frequency Based on Resolved Atmospheric Patterns.** *Gao et al., Oct 2016*

301. **Combining Price and Quantity Controls under Partitioned Environmental Regulation.** *Abrell & Rausch, Jul 2016*

300. **The Impact of Water Scarcity on Food, Bioenergy and Deforestation.** *Winchester et al., Jul 2016*

299. **The Impact of Coordinated Policies on Air Pollution Emissions from Road Transportation in China.** *Kishimoto et al., Jun 2016*

298. **Modeling Regional Carbon Dioxide Flux over California using the WRF-ACASA Coupled Model.** *Xu et al., Jun 2016*

297. **Electricity Investments under Technology Cost Uncertainty and Stochastic Technological Learning.** *Morris et al., May 2016*

296. **Statistical Emulators of Maize, Rice, Soybean and Wheat Yields from Global Gridded Crop Models.** *Blanc, May 2016*

295. **Are Land-use Emissions Scalable with Increasing Corn Ethanol Mandates in the United States?** *Ejaz et al., Apr 2016*

294. **The Future of Natural Gas in China: Effects of Pricing Reform and Climate Policy.** *Zhang & Paltsev, Mar 2016*

293. **Uncertainty in Future Agro-Climate Projections in the United States and Benefits of Greenhouse Gas Mitigation.** *Monier et al., Mar 2016*

292. **Costs of Climate Mitigation Policies.** *Chen et al., Mar 2016*

291. **Scenarios of Global Change: Integrated Assessment of Climate Impacts.** *Paltsev et al., Feb 2016*

290. **Modeling Uncertainty in Climate Change: A Multi-Model Comparison.** *Gillingham et al., Dec 2015*

MIT Joint Program on the Science and Policy of Global Change

Massachusetts Institute of Technology
77 Massachusetts Ave., E19-411
Cambridge MA 02139-4307 (USA)

T (617) 253-7492 **F** (617) 253-9845
globalchange@mit.edu
http://globalchange.mit.edu/